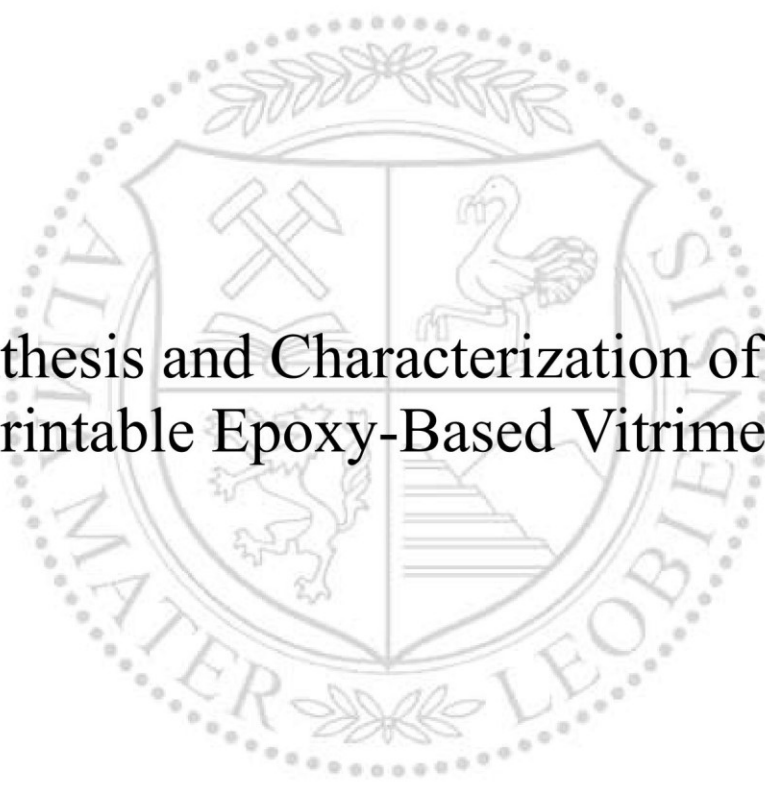




Chair of Chemistry of Polymeric Materials

Master's Thesis



Synthesis and Characterization of 3D-  
Printable Epoxy-Based Vitrimers

Rita Johanna Höller, BSc

November 2022



**EIDESSTÄTTLICHE ERKLÄRUNG**

Ich erkläre an Eides statt, dass ich diese Arbeit selbständig verfasst, andere als die angegebenen Quellen und Hilfsmittel nicht benutzt, und mich auch sonst keiner unerlaubten Hilfsmittel bedient habe.

Ich erkläre, dass ich die Richtlinien des Senats der Montanuniversität Leoben zu "Gute wissenschaftliche Praxis" gelesen, verstanden und befolgt habe.

Weiters erkläre ich, dass die elektronische und gedruckte Version der eingereichten wissenschaftlichen Abschlussarbeit formal und inhaltlich identisch sind.

Datum 18.11.2022

*Rita Johanna Höller*

Unterschrift Verfasser/in  
Rita Johanna Höller

## **Acknowledgements**

The research work was performed within the COMET-Module project "Chemitecture" (project-no.: 21647048) at the Polymer Competence Center Leoben GmbH (PCCL, Austria) within the framework of the COMET-program of the Federal Ministry for Transport, Innovation and Technology and the Federal Ministry for Digital and Economic Affairs with contributions by Montanuniversitaet Leoben (Institute of Chemistry of Polymeric Materials). The PCCL is funded by the Austrian Government and the State Governments of Styria, Lower Austria and Upper Austria.

First and foremost, I would like to thank Priv.-Doz. Dipl.-Ing. Dr. Sandra Schlögl for the supervision of this thesis and for enabling many new experiences along the way. Thank you for always being so supportive and encouraging as well as providing a motivating working environment.

Next, I would like to sincerely thank Dr. mont. Dipl.-Ing. Elisabeth Rossegger for her patience and her dedicated support and supervision over the last years.

Further, I want to thank everyone at PCCL and the Institute of Chemistry of Polymeric Materials at Montanuniversitaet Leoben for the pleasant work climate and their helpfulness in general. I especially owe thanks to David Reisinger for many helpful conversations and the rheometer measurements, to Walter Alabiso who did all DMA measurements, to Florian Wanghofer for the TGA measurements and to Evelyn Sattler for the tensile testing.

Last but not least, I would like to sincerely thank my family and also my friends for the continuous support over the past years – Danke!

## Kurzfassung

Der 3D-Druck von Photopolymeren ist eine Fertigungstechnologie, die Möglichkeiten für viele verschiedene Anwendungen bietet, wie etwa für Soft Robotics, Rapid Tooling oder auch für die Biomedizin. Viele der für den 3D-Druck verwendeten Harze basieren jedoch auf Acrylaten, die aufgrund ihres Vernetzungsmechanismus zu Polymernetzwerken mit schlechten mechanischen Eigenschaften (u.a. geringe Zähigkeit) führen. Diese Charakteristika schränken die Nutzung des 3D-Drucks vor allem in Bereichen wie dem Rapid Tooling ein, wo häufig zähe Materialien erforderlich sind. In der vorliegenden Arbeit wurde versucht, die hervorragende Druckbarkeit von Acrylatharzen mit den überlegenen mechanischen Eigenschaften von Epoxidharzen zu kombinieren, um diese Einschränkungen zu überwinden. Durch die Herstellung eines Polymermaterials, welches aus zwei interpenetrierenden Netzwerken besteht, wird die Verarbeitung mittels 3D-Druck und anschließender thermischer Aushärtung möglich. Darüber hinaus wurden in dieser Arbeit hohe Glasübergangstemperaturen sowie vitrimere Eigenschaften angestrebt. Vitrimere weisen bei erhöhten Temperaturen katalysierte Austauschreaktionen zwischen kovalenten Bindungen auf, wodurch die Netzwerke Spannungsrelaxation, Heilung oder sogar Recycling erfahren können.

Im Rahmen dieser Arbeit wurde ein 3D-druckbares Harz mit vitrimeren Eigenschaften entwickelt, das auf einem Acrylat- und einem Epoxid-Anhydrid-Netzwerk basiert. Die Materialeigenschaften wurden im Detail charakterisiert und durch Variation des Verhältnisses von Acrylat- und Epoxid-basierten Harzkomponenten konnten weitere Erkenntnisse über das Materialverhalten gewonnen werden. Die thermischen Eigenschaften wurden mittels thermogravimetrischer Analyse und dynamisch-mechanischer Analyse bestimmt. Weiters wurde das Aushärtungsverhalten mittels dynamischer Differenzkalorimetrie und Fourier-Transform-Infrarotspektroskopie untersucht. Zusätzlich wurden Spannungsrelaxationsexperimente und Zugversuche zur Bewertung der mechanischen Eigenschaften durchgeführt. Das in dieser Arbeit optimierte Harz weist nach zwei Aushärtungsschritten – 3D-Druck nach dem Prinzip der digitalen Lichtverarbeitung und anschließender thermischer Härtung – eine hohe Glasübergangstemperatur (112 °C) auf. Infolge seiner thermischen und mechanischen Eigenschaften ist das hergestellte Material ein vielversprechender Kandidat für den Einsatz im Rapid Tooling.

## **Abstract**

3D-printing of photopolymers is a technology that offers possibilities for numerous applications, such as soft robotics, rapid tooling or biomedical devices. However, many resins used in 3D-printing rely on acrylates – entailing polymer networks with poor mechanical properties (e.g. low toughness) due to their crosslinking mechanism. Those features limit the utilization of 3D-printing especially in fields such as rapid tooling, where tough materials are necessary. The thesis at hand sought to combine the excellent printability of acrylic resins with the superior mechanical properties of epoxy resins in order to overcome those limitations. The creation of a polymer material, consisting of two interpenetrating networks, makes a processing through 3D-printing and subsequent thermal curing possible. Additionally, this thesis aimed at achieving high glass transition temperatures as well as vitrimeric properties. Vitrimers exhibit catalyzed exchange reactions between covalent bonds at higher temperatures, enabling them to undergo stress relaxation, healing or even recycling.

In the course of this thesis, a 3D-printable resin with vitrimeric properties was developed based on an acrylate and an anhydride-epoxy network. Material properties were analyzed and by varying the ratios of acrylate-based and epoxy-based resin components, further insights into material behavior were gained. Thermal properties were determined through thermogravimetric analysis and dynamic mechanical analysis. Curing behavior was examined using differential scanning calorimetry and Fourier-transform infrared spectroscopy. Additionally, stress relaxation experiments and tensile testing were used to assess mechanical properties. The optimized resin exhibited a high glass transition temperature (112 °C) after undergoing digital light processing and thermal post-curing. Altogether the material developed is a promising candidate for applications in rapid tooling due to its thermal and mechanical properties.

# Table of Contents

<b>1</b>	<b>INTRODUCTION</b>	1
<b>2</b>	<b>THEORY</b>	3
2.1	PHOTO-INDUCED BOND FORMATION	3
2.1.1	Radically Induced Chain Growth Polymerization	6
2.2	THERMALLY INDUCED RING OPENING POLYMERIZATION	11
2.2.1	Thermally Induced Anionic Ring Opening Polymerization (Epoxy-Anhydride Networks)	14
2.3	INTERPENETRATING POLYMER NETWORKS	18
2.3.1	Dual-Curing	20
2.4	VITRIMERS	22
2.5	3D-PRINTING	26
2.5.1	Possible Applications – Rapid Tooling	28
<b>3</b>	<b>EXPERIMENTAL</b>	31
3.1	CHEMICALS	31
3.2	DEVICES	32
3.3	PREPARATION OF THE RESINS	32
3.4	3D-PRINTING AND THERMAL CURING	33
3.5	FTIR-MEASUREMENTS	34
3.6	DYNAMIC MECHANICAL ANALYSIS	35
3.7	DIFFERENTIAL SCANNING CALORIMETRY	35
3.8	STRESS RELAXATION	36
3.9	SWELLING MEASUREMENTS	36
3.10	TENSILE TESTING	36
3.11	THERMOGRAVIMETRIC ANALYSIS	37
<b>4</b>	<b>RESULTS AND DISCUSSION</b>	38
4.1	CURING OF THE RESINS	39
4.1.1	Differential Scanning Calorimetry	39
4.1.2	Fourier-Transform Infrared Spectroscopy	42
4.2	THERMAL PROPERTIES	47
4.2.1	TGA Measurements	47
4.2.2	DMA Measurements	49
4.3	CROSSLINKING DEGREE – SWELLING EXPERIMENTS	53
4.4	MECHANICAL PROPERTIES	55
4.4.1	Stress Relaxation	55
4.4.2	Tensile Testing	60
<b>5</b>	<b>SUMMARY AND OUTLOOK</b>	62
<b>6</b>	<b>LITERATURE</b>	64
<b>7</b>	<b>ABBREVIATIONS AND SYMBOLS</b>	70
<b>8</b>	<b>LIST OF TABLES</b>	73
<b>9</b>	<b>TABLE OF FIGURES</b>	74

# 1 Introduction

The advent of additive manufacturing has entailed a multitude of applications and possibilities across many fields of research. Among the different additive manufacturing technologies 3D-printing holds a special position, as it has the potential to become a very important method for polymer processing. This is due to many advantageous features, such as high flexibility, a variety of customization possibilities, and last but not least a reduced amount of waste. In times of high awareness for environmental issues, the latter is of special importance – although minimizing excess material also has economic benefits. By combining 3D-printing and photopolymerization, it becomes possible to achieve not only control over mechanical and chemical features but also high printing resolutions [1]. In order to enable even more opportunities, vitrimeric materials can be introduced to 3D-printing. Vitrimers can experience stress relaxation, shape memory abilities, and recyclability due to dynamic exchange reactions between covalent bonds. Those reactions are typically promoted by high temperatures and catalysts [2].

One of the many applications of 3D-printing is rapid tooling – producing tools that can be used directly via 3D-printing. Injection molding or extrusion are both prominent routes for polymer processing, but both have the disadvantage of fairly high tooling costs. In particular during developmental stages of production, rapid tooling has great potential to make the process faster (short production times) and significantly cheaper (low investment costs). Obviously, not all 3D-printable materials can be used for rapid tooling – especially not all polymeric materials. They need to exhibit thermal stability above the processing temperatures of the respective fabrication route as well as mechanical properties that withstand the high pressures [3].

This thesis aims at developing vitrimeric photopolymerizable materials with high thermal stability that can be processed through 3D-printing but also contain thermally curable epoxy resins. Approaching this task, an interpenetrating combination of an acrylic and an epoxy-anhydride network is produced. Dual curing – digital light processing 3D-printing followed by a thermal post-curing step is utilized to enable polymerization for both networks. The effects of the respective amount of acrylate and epoxy-anhydride resin are studied by varying the ratios of said components from 50:50 to 80:20 (epoxy-anhydride : acrylate). In order to evaluate the curing behavior of the resins prepared, Fourier-transform infrared spectroscopy and differential scanning analysis are used. From those measurements it is possible to

## 1. Introduction

---

determine processability. Dynamic mechanical analysis is employed to analyze the glass transition temperatures ( $T_g$ ) of the different materials, as another goal of this work is reaching a high  $T_g$  ( $> 100$  °C). Thermal stability is assessed through thermogravimetric analysis and swelling experiments provide further insight into the crosslink density of the networks obtained. Evaluating vitrimeric behavior is realized by conducting stress relaxation measurements. Additionally, tensile testing is utilized to gain information about the mechanical properties of the resin materials.

Finally, the material presented in this thesis exhibits a glass transition temperature above 110 °C and further promising thermal properties. The network performs well in mechanical testing – stress relaxation and tensile testing – too. As a result, it should be considered to be a candidate for applications in rapid tooling – especially in the processing of elastomers.



# 2 Theory

## 2.1 Photo-induced Bond Formation

Photochemistry has proven to be a very valuable way to synthesize molecules and functional polymers over the past decades. Possible applications range from dental fillings, coatings, bonding agents, inks, micro-electronics to 3D-printing and many more [4]. Light can be used effectively to design properties, structure and even the shape of a material itself. In these processes, the use of light offers three major advantages over other approaches and, in particular, thermally induced reactions. Most importantly, reactions that would require high temperatures can be carried out using photoinitiation as an energy source. This is based on the fact that the energy input that photons contribute to a reaction is 130 to 190 times higher than the thermal energy input at room temperature, depending on the wavelength of the radiation. The second favorable aspect of photoinitiation is that temporal control over the reaction is feasible by removing the light source – also the start of the process can be set very precisely through switching on irradiation. Thirdly, reactions triggered by light can additionally be spatially controlled. By applying a pattern during irradiation, e.g., through a mask or a digital light projector, reactions are controlled two-dimensionally. Combining temporal and spatial control enables techniques such as stereolithography/additive manufacturing or photoresist technology [4, 5].

Three different types of photo-induced reactions are distinguished: formation of bonds, isomerization reactions and breaking of bonds. Bond formation can occur in different ways – either with or without the use of a photo-initiator. To avoid the use of a photo-initiator, molecules bearing chromophore moieties are required that are able to react with each other directly [5, 6].

The basic principle of photo-triggered reactions is the absorption of a photon by a molecule. Two laws were formulated to provide a foundation: First, the Grotthus-Draper-law states that only light absorbed by a chemical compound can lead to a photochemical reaction. Secondly, the so-called Stark-Einstein law claims that each absorbed photon initiates the photoreaction of exactly one molecule.

According to Planck's law, the energy  $E$  of a photon can be expressed via the following equation, with  $h$  being the Planck's constant and  $\nu$  the oscillation frequency of the photon:

$$E = h\nu$$

## 2. Theory

In chemical equations, the arithmetic expression ' $h\nu$ ' is regularly used to symbolize a photon. As soon as a molecule absorbs a photon, its energetic state changes from ground-state ( $S_0$ ) to electronically excited state. More precisely, the distribution of electrons within the molecular orbitals is changed. A distinction is made between the highest occupied molecular orbital (HOMO) and the lowest unoccupied molecular orbital (LUMO). When photo-irradiation occurs, i.e., a photon with the required energy is absorbed, an electron migrates from the HOMO to the LUMO, resulting in an excited state ( $S_1$ ), as **Error! Reference source not found.** i

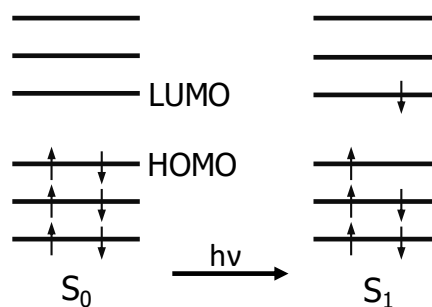


**Figure 1: HOMO - LUMO - transition (adapted from [8])**

illustrates.

Obviously, the spectrum of the incident radiation and the absorption spectrum must overlap significantly. Different types of lamps or even lasers can be used to emit light [7, 8].

Numerous equations have been established to describe this process, for example the Beer-Lambert law, expressing the absorption of light by one individual absorbing molecule

$$A = \varepsilon cd = -\log\left(\frac{I}{I_0}\right)$$

with  $A$  being the absorbance of irradiation inside a film,  $d$  the length of the optical path,  $\varepsilon$  the molecular extinction coefficient,  $c$  the concentration of the absorbing moiety,  $I$  the emergent intensity and  $I_0$  the incident intensity of irradiation. As soon as more than one light-absorbing species is present,  $A$  becomes the sum of absorption values for each species. To determine the total absorbed intensity  $I_A$ , the difference between incident and emitted intensity is calculated:

$$I_A = I_0 - I$$

Every photochemical process needs a certain quantity of absorbed photons, represented by a wavelength dependent quantum yield  $\varphi$ . Hence, the rate of initiation for a specific photo-triggered reaction –  $R_i$  – with only one absorbing species amounts to:

## 2. Theory

$$R_i = \varphi I_A = \varphi(I_0 - I)$$

These equations show that fast reaction rates require sufficiently high absorption of light. While in clear materials and thin films light can consistently reach the whole geometry, especially thick films and opaque materials with high absorption can drastically limit the area affected by light. This phenomenon leads to the formation of gradients in material properties, which is often a decisive disadvantage. To give an example: in manufacturing techniques such as 3D-printing the range of the incident light must be taken into account in order to obtain objects with uniform properties [5].

So-called Jablonski diagrams are used for the visual representation of molecules in the excited state. These diagrams depict transitions between the different energy states of a molecule as well as the attainment of the excited state and the ground state. A schematic Jablonski diagram is shown in Figure 2: schematic Jablonski diagram (adapted from [7]). Abbreviations:

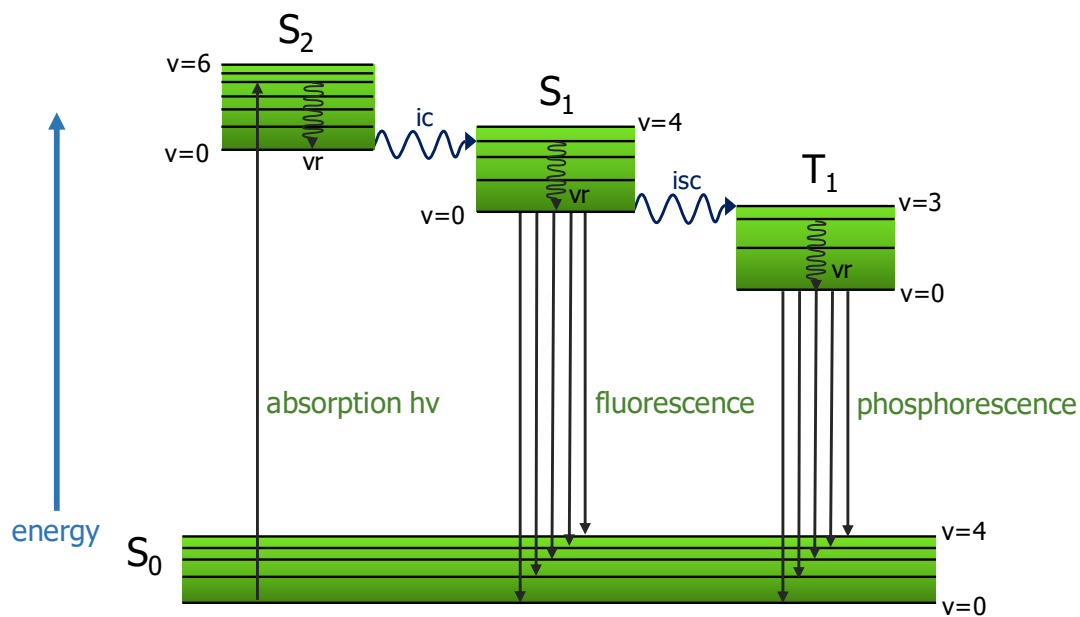


**Figure 2: schematic Jablonski diagram (adapted from [7]). Abbreviations: ic - internal conversion; isc - intersystem crossing; vr - vibration-relaxation**

ic - internal conversion; isc - intersystem crossing; vr - vibration-relaxation.

The diagram above shows the different pathways of deactivation that a molecule can undergo in the excited state. After absorbing a photon, the molecule changes from ground state ( $S_0$ ) to excited state ( $S_2$ ) and subsequently undergoes several photophysical processes to leave the usually rather short-lived excited state. Radiationless vibrational relaxation ( $vr$ ) causes the vibrational state to drop from  $v=4$  to  $v=0$  while remaining in the same electronic state ( $S_2$ ).

## 2. Theory

---

Via an internal conversion process (ic), that is again radiation-free, another excited state ( $S_1$ ) is isoenergetically achieved. From there, in addition to vibrational relaxation, two possibilities can be observed, namely fluorescence, a radiative process leading back to  $S_0$ , and intersystem crossing, which is spin-forbidden and results in the triplet state  $T_1$  (see Figure 2). Following vibrational relaxation, the molecule reaches  $S_0$  again via phosphorescence, a radiative process, through emitting a photon [7].

Ultimately, there are many advantages to photo-induced bond formation, including less side reactions compared to thermally induced bond formation, or low polymerization temperatures. Oftentimes, photochemistry also leads to "greener" reactions, as no solvents have to be used. This enables complex applications such as dental fillings or coatings, as well as additive manufacturing or UV-curable inks [4, 5].

### 2.1.1 Radically Induced Chain Growth Polymerization

This chapter focuses on the radically induced chain growth reaction as it is a common pathway for acrylate homopolymerization. Free radical polymerization is usually induced by a photo-initiator, of which there are two main types: On the one hand, there are Type I systems. They consist of a singular molecule that, when irradiated, generates two radicals – each of which can trigger a reaction in most cases. On the other hand, there are Type II systems that feature a bimolecular reaction. Here, a radical is formed when the photochemically excited state of one molecule undergoes an interaction with the second molecule in the ground state. When selecting a photo-initiator for a system that polymerizes via a free-radical pathway, several factors have to be considered: solubility in the respective monomers, yellowing, financial and availability aspects, curing speed and last but not least the absorption wavelength range of the initiator [4, 5].

Type I photo-initiators are mainly chemicals bearing an aromatic carbonyl moiety; for instance benzoin including its derivatives, acetophenones, aminoalkyl phenones, benzyl ketals,  $\alpha$ -hydroxyalkyl ketones, O-acyl- $\alpha$ -oximino ketones, and phosphine oxides. All of these compounds decompose into radicals upon irradiation via  $\alpha$ -cleavage. Among them, benzoin exhibits high efficiency and reactivity – making it and its derivatives the most widely used photo-initiators for free radical polymerization. Its thermal instability due to the benzylic hydrogen that can be abstracted however leads to reduced shelf life. Another downside to benzoin and its derivatives is the yellowing of cured material, as well as its poor ability to absorb light in the near UV region. If thermal stability is sought, phosphine oxides are a good choice, additionally

## 2. Theory

---

also possessing high reactivity. Their molecular structure enables the monomers to react with the formed radical under favorable steric conditions. Furthermore, they undergo photobleaching – which means their reaction yields byproducts that are UV-transparent – leading to a higher light penetration depth and the absence of yellowing. Common examples of phosphine oxide photo-initiators are bis(2,4,6-trimethylbenzoyl)-phenylphosphine oxide

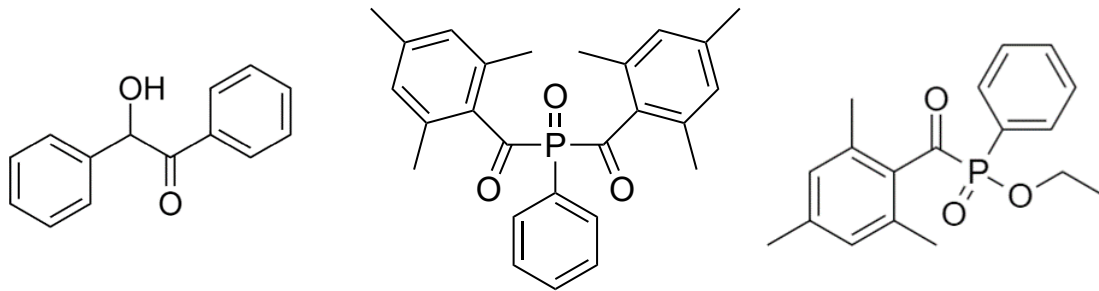


**Figure 3: molecular structures of benzoin, BAPO, and TPO-L (from left to right)**

(BAPO) or ethyl (2,4,6-trimethylbenzoyl)-phenyl phosphinate (TPO-L). Those initiators absorb light well in the near UV area of the spectrum, making them attractive for many industrial applications. The structures of benzoin, BAPO and TPO-L are shown in Figure 3 [4, 9–11].

Norrish type II photoinitiators proceed more slowly in their radical-generating phase, as the reaction is bimolecular. This mechanism also slows down the curing rate. Photolytic cleavage of aromatic ketones – for instance benzophenone, quinones and thioxanones – produces ketyl radicals if the reaction occurs in the presence of a hydrogen donor, as well as a second radical derived from the hydrogen donor. Several aspects must be considered in this bimolecular reaction: Firstly, additives are often required due to the chain terminating effect of ketyl radicals on the polymerization. Secondly, ketyl radicals entail steric hindrance as well as an unpaired electron, leading to a very unreactive behavior regarding vinyl monomers. Further, the abstraction of hydrogen from the donor molecule must combat numerous side reactions. Therefore, it is vital to choose a H-donor that reacts rapidly with the irradiated, excited photoinitiator molecule. Obviously, there are also many type II photo-initiator systems available [4, 12].

Once a photo-initiator system with a suitable light source has been found, the first step towards initiating a free-radical induced polymerization reaction has been taken. In the following paragraphs, the mechanisms of free radical chain growth polymerization will be discussed.

As soon as radicals generated by the photoinitiator are available, they react with a monomer to form a new reactive species. Figure 4 depicts this process, including the next steps, one of which is chain propagation – when the growing chain reacts with additional monomer

## 2. Theory

molecules to form a polymer. As soon as a reaction takes place between two reactive species, termination of the polymerization reaction is the result. A reactive chain or a radical can also react with the polymer leading to branching, which is not illustrated here [4, 13].

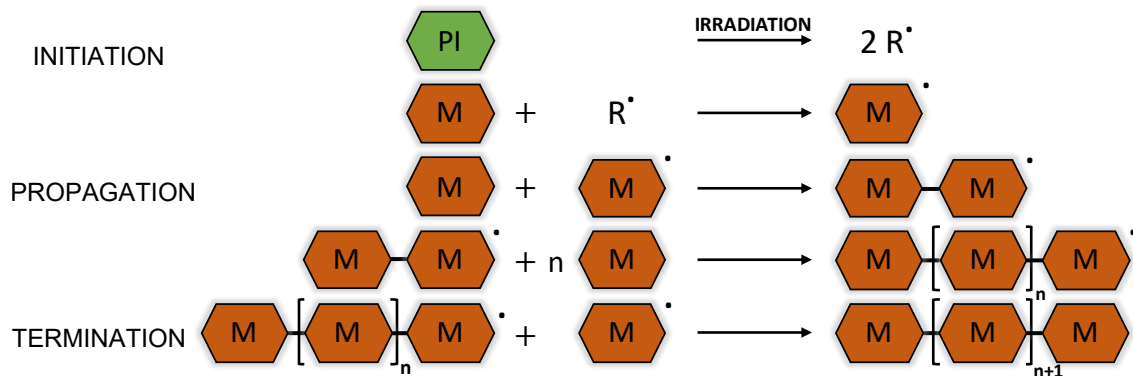


**Figure 4: scheme of a chain growth polymerization**

As radical chain growth polymerization usually proceeds very swiftly, the mass of the polymer chains also grows quite rapidly. This results in a shift from liquid to solid phase within a matter of seconds. In order to detect the degree of polymerization, methods such as measuring the monomer conversion via Fourier transform infrared spectroscopy (FTIR) are applied. Obviously, the length of the polymer chain, molecular weight and crosslink density change with monomer conversion. Therefore, other material properties, such as volume shrinkage, Young's modulus or glass transition temperature ( $T_g$ ) are also influenced by the rapid changes. If the volume shrinkage is too high, warpage due to residual stresses can be the result [14, 15].

Polyacrylates frequently pose as an example for free radical polymerization. Acrylate monomers are usually esters derived from acrylic acid, but there are also methacrylates, cyanoacrylates and some others. Low-molecular weight esters are usually produced by esterification, while higher-molecular ones are prepared by ester exchange [16]. The structures of an exemplary acrylate and glycerol 1,3-diglycerol diacrylate, which was used in this work, are shown in Figure 5.

## 2. Theory

---

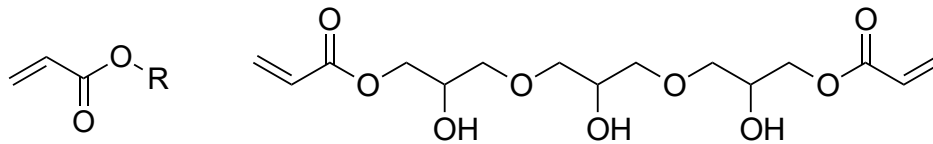


**Figure 5: chemical structures of a generic acrylate (left) and of glycerol 1,3-diglycerolate diacrylate (right)**

Even though polyacrylates have been (and still are) used commercially for some time, e.g., as coatings, paints or adhesives, it has taken science a while to understand the reaction mechanisms in detail [13]. During the polymerization reaction, a transfer of the active radical to the polymer happens regularly – intermolecularly as well as intramolecularly. As a consequence, two different forms of radicals exist: the so-called secondary propagating radical and the tertiary mid-chain radical [17]. These rather unreactive mid-chain radicals mainly stem from intramolecular transfer, also known as backbiting. Due to the stability and slow reaction rates of the tertiary radical, their number increases in the course of polymerization. Accordingly, the microstructure of the emergent polymer is influenced as branching and cross-linking lead to a variety of polymer structures – which of course also effects the material properties such as  $T_g$ , for instance [13, 18].

Another problematic phenomenon in radical polymerization is volumetric shrinkage, as mentioned above. Overly fast chain growth and the resulting solidification of the resin are the cause of this phenomenon that affects not only acrylates but also other free radical chain growth processes. On the one hand, residual stresses, that lead to warpage and distortion of the produced shape, are problematic. On the other hand, the precision of the measurements is negatively affected by shrinkage. This is a major downside of acrylate homopolymerization, especially in applications such as 3D-printing [4, 15].

Last but not least, oxygen inhibition is also a drawback in acrylate polymerization and radical polymerization in general. Oxygen is able to react with radicals of all sorts – photo-initiator, propagating chain ends and also initial monomer radicals – and thus quenching their reactivity. Resulting peroxy radicals usually recombine, which ends the polymerization process. Effects ensuing from oxygen inhibition are insufficient curing, sticky surfaces and sometimes curing is not feasible at all. Curing reactions usually take place under ambient air which makes the influence of oxygen a widespread problem [19].

Different approaches, such as combining acrylates with thiols have been tested to improve shape retention as well as oxygen inhibition [20].

## 2. Theory

---

Despite drawbacks such as irregular structures, shrinkage and oxygen inhibition, free radical polymerization nevertheless finds many uses – but also because it uses the disadvantages to achieve new effects [5].



### 2.2 Thermally Induced Ring Opening Polymerization

The following chapter serves as an introduction to ring opening polymerization. As the name implies, the monomers here have ring structures – such as cyclic esters, amides or ethers, to be precise – which are broken during the reaction process.

Since many different cyclic molecules are available, there are two main factors that determine whether or not a molecule is polymerizable through ROP. Most dominant is the thermodynamic factor, being a comparison of the stability of the cyclic monomer and the respective linear one. Comparing ring molecules of different sizes, polymerization seems to be the preferred route for all but six-membered rings. However, the thermodynamic factor does not solely determine if a cyclic molecule can be polymerized; there is also the kinetic factor. Cycloalkanes for example cannot undergo ROP due to kinetic reasons – in contrast to cyclic ethers, lactones and others. Their heteroatoms within the ring serve as an attack site for nucleophilic or electrophilic species, enabling initiation and subsequent propagation of the polymer chain. Generally, cyclic monomers with 3,4 or 7-11 ring atoms undergo ROP more readily [14].

Ionic ROP can be initiated via a cationic or an anionic mechanism. Initiating molecules for anionic ROP are nucleophiles, including organometals, metal amides, phosphines, amines or water for instance [21]. An active center is the result of initiation and gives way to propagation – adding monomers to the active center, which is renewed after each addition [22]. Most monomers are able to either undergo cationic or anionic ROP. Ethers for example usually undergo cationic polymerization, but epoxides are polymerizable via both pathways, owing to their high ring strain [14]. Their structure allows both the oxygen being attacked electrophilically and the carbon atoms to be submitted to nucleophilic attack [22].

Comparing ionic ROP to the free radical chain growth mechanism of acrylates, which was described thoroughly in chapter 2.1.1, oxygen inhibition does not pose a problem for ionic polymerization. Oxygen reacts with radicals, quenching them and in the process hindering the progress of chain growth. As there are no radicals involved in ionic ROP, it is insensitive to oxygen and can therefore proceed at ambient conditions and under air without interference [19]. Additionally, there are significantly fewer side reactions during ionic ROP – especially when talking about the curing of epoxy resins – than for the free radical polymerization of acrylates. Therefore, the network structure originating from ionic ROP is more homogenous than it is the case for acrylates, which have the disadvantage of irregular buildup [21]. Finally, high shrinkage is often mentioned as an unfortunate property of radically polymerized acrylates. Caused by the ring opening mechanism during the curing of epoxy

## 2. Theory

---

resins (and other chemicals used in ROP), the materials produced exhibit much less shrinkage as the monomers are broken up from their cyclic form [4, 22].

Having already been mentioned a few times in the preceding paragraphs, epoxides are a very prominent example for molecules that undergo ROP. Epoxy resins have been in use for a long time, as the earliest products were manufactured in the 19<sup>th</sup> century already. In the 1940s, the first introduction of commercial epoxy resins to the US-market took place. Since then, the variety of epoxy resin systems available has increased enormously, making them vital for many industrial applications. Due to their relatively high pricing, they mainly find use in technically advanced utilizations [23].

Besides the afore mentioned photocured acrylate network, epoxy resin was the second large component of the materials created in this thesis. Chemically, epoxy is the trivial name of the 3-membered cyclic ether. Figure 6 shows the structure of a generic epoxy as well as the chemical structures of the two resins used during the experimental part of this thesis.

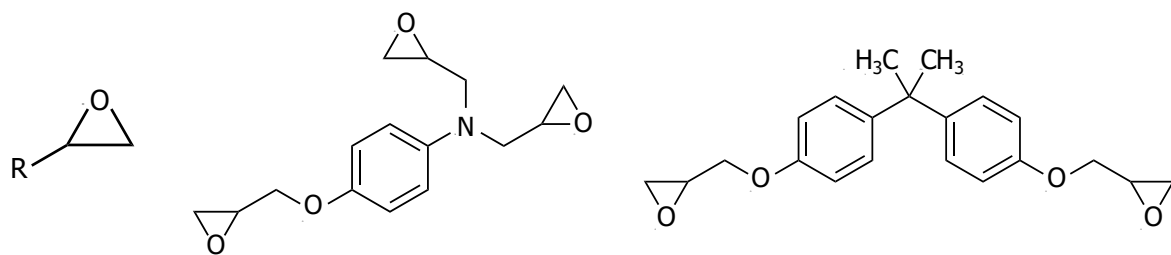


**Figure 6: general structure of an epoxy group (left) and *N,N*-diglycidyl-4-glycidyl-aniline (DGOA, middle) and bisphenol-A-diglycidyl-ether (right), both epoxies used in this thesis**

There being a wide variety of different epoxy monomers, a classification into subgroups has been made over time. Epichlorohydrin and bisphenol-A are the educts for the most commonly used class of epoxy monomers – diglycidyl ethers of bisphenol-A, or short DGEBA (shown in Figure 6 on the right). DGEBA-type materials amount to approximately 80-85 % of the globally used epoxy resins. Further subgroups of epoxy resins are brominated resins, novolac resins, phenoxy resins and cycloaliphatic resins. In addition to those mainly used monomers, there are also many specialty resins, for instance multifunctional epoxies. Although their market volume is significantly lower than for the above-mentioned resin groups, they are especially valued in research and development. The mainly used epoxy monomer in this thesis also belongs to these multifunctional epoxies (seen in Figure 6 in the middle) [23, 24].

## 2. Theory

---

As soon as epoxy resins are cured, they are identified as thermosetting polymers, as they exhibit a highly crosslinked structure. Therefore, they cannot be melted and possess characteristics such as high – crosslink-density-dependent -  $T_g$  and low flexibility. Nowadays, epoxy resins are used in applications such as coatings, electrical and electronical uses (e.g., insulation) and many more [24].

Creating networks – thermosetting polymers – from epoxy monomers is termed curing and utilizes crosslinking agents, often also referred to as hardeners or curing agents. There are catalytic hardeners that promote homopolymerization or multifunctional curing agents. Chemicals such as amines, anhydrides or acids are conventionally used curing agents [24].

Homopolymerization of epoxy bearing molecules is possible as well and mainly applied in the cationic photochemical curing of epoxides. It mainly takes place in mixtures with an excess of epoxy and at high temperatures – the reaction mechanism, an etherification, is pictured in Figure 7. It should be noted that OH-groups catalyze the homopolymerization reaction. Often, also other catalytic curing agents are used in order to achieve homopolymerization at lower temperatures – the high reaction temperatures otherwise consume a lot of energy [22, 25, 26].

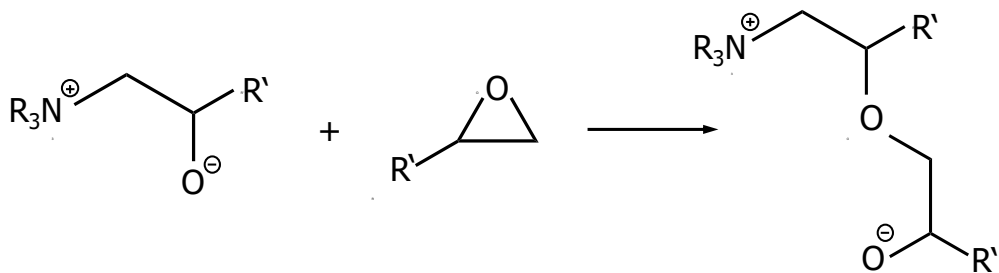


**Figure 7: epoxy homopolymerization – etherification reaction between alkoxide ion and epoxy molecule**

Generally speaking, ring opening polymerization can proceed via different routes for epoxides. One possibility is step growth polymerization, where two different functional groups react with each other to form a polymer. To give an example, curing of epoxides with multifunctional primary amines proceeds via step growth. Another pathway is chain growth polymerization – ionic ring opening polymerization to be more precise. [22]

## 2. Theory

### 2.2.1 Thermally Induced Anionic Ring Opening Polymerization (Epoxy-Anhydride Networks)

This chapter will focus on the anionic ROP. It is important to note that the curing reaction of epoxides via anionic ROP is activated thermally and takes place at elevated temperatures usually (well) above 100 °C [23, 27]. Figure 8 illustrates the polymerization steps, starting with a nucleophilic molecule ("Nuc<sup>-</sup>") and the heterocyclic monomer. The functional group within the cyclic monomer is polar and symbolized by X – Y, where X is normally an electron-deficient carbon atom and Y an electron-withdrawing atom, e.g., nitrogen or oxygen. By the nucleophilic molecule attacking X the monomer ring is opened, leading to a negatively charged Y on the other end, which is able to attack another monomer. Hence, through adding monomer after monomer, a polymer is formed at the end of the chain growth-like process [21, 28].

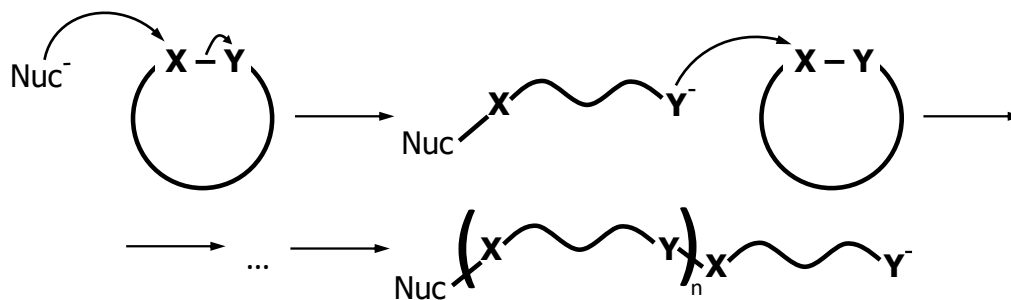


**Figure 8: general mechanism of anionic ROP, adapted from [21]**

A stellar feature of ionic ROPs and especially the anionic polymerization of epoxides is their capability to create block copolymers. Being made possible by the so-called "living polymerization" – a lack of termination reactions – this trait is useful in a number of applications. The negatively charged active chain end persists until it is neutralized [14].

During the curing of epoxy resins, usually curing agents are utilized. Multifunctional amines experience the most interest as crosslinkers currently, but they have an inherent disadvantage: polar groups produced during curing lead to high water absorption rates and compromise the final material's properties as a consequence. To circumvent this, carboxylic acid anhydrides can be used. Networks obtained from the reaction between epoxy and anhydride showcase properties such as low internal stresses, low shrinkage, high  $T_g$  and remarkable insulating qualities for electrical applications. In most cases, the curing reaction is not taking place at room temperature but at elevated temperatures above 120 °C – leading to rather high production costs [24].

## 2. Theory

---

Figure 9 illustrates the general structure of a carboxylic acid anhydride and the cyclic anhydride used during the experimental work of this thesis. Like the majority of relevant anhydrides, also methyl nadic anhydride (MNA) is cyclic. MNA promotes rigidity due to the rather stiff cycloaliphatic rest of the molecule [23].

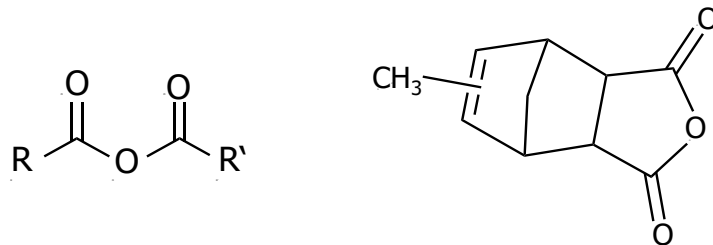


**Figure 9: general structure of a carboxylic acid anhydride (left) and structure of methyl-5-norbornene-2,3-dicarboxylic anhydride (MNA) (right)**

Generally speaking, there is not only one curing mechanism for epoxy-anhydride systems. Due to the complexity of the processes occurring, there have been many different studies over the years and especially the initiation mechanism was subject to many postulated theories [29]. In the case of an uncatalyzed curing reaction, an availability of hydroxyl groups is necessary for initiation. They attack the molecule with the anhydride group, thus opening the ring and forming an ester group and a carboxylic acid group. The latter is able to react with an epoxy monomer resulting in the newly emergent molecule to have two ester groups and a free hydroxyl group. From here on, there are two possibilities for the reaction to proceed: the addition of another anhydride molecule via an esterification reaction or the addition of an epoxy molecule, forming an ether link [23, 24]. Functional groups reacting with each other being the cause for chain growth, the mechanism here can be identified as a polyaddition reaction [25].

Usually though, the curing of epoxy resins with anhydrides is accelerated using Lewis bases, e.g., tertiary amines, ammonium salts or imidazoles. As Figure 6 shows, DGOA possesses not only three epoxy groups but also a tertiary amine and is therefore able to act as an initiator. The reaction route via tertiary amine acceleration leads to anionic polymerization. Overall, there have been a number of theories regarding the mechanism of initiation. The consensus nowadays is that a zwitterion, i.e. a molecule that bears two functional groups where one of them is charged positively and the other one negatively, is created [22, 25, 30]. Within this reaction of the tertiary amine with an epoxy monomer, the two groups originating are an alkoxide (negative) and a quaternary nitrogen (positive), as illustrated in Figure 10 **Error! Reference source not found.** [31].

## 2. Theory

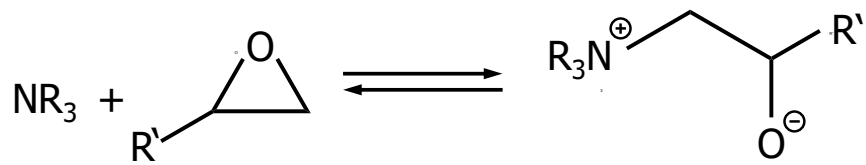


**Figure 10: formation of a zwitterion from the reaction of epoxide with tertiary amine**

The newly created alkoxide moiety is now the active center for an anionic polymerization, which progresses as apparent in Figure 11. It is shown that an anhydride molecule is attacked by the negatively charged alkoxide group, thus its ring structure is opened and a new molecule bearing a carboxylate moiety is generated. Subsequently, this emergent ester containing molecule is able to attack an epoxy molecule via its carboxylate group in a ring opening reaction, and hence propagates chain growth – a process which is pictured in Figure 12. Generating another alkoxide group within the course of the reaction, a further anhydride bearing molecule is quickly bound to the growing chain – which in turn enables the addition of an epoxy molecule via the newly originated carboxylate anion [23, 24].

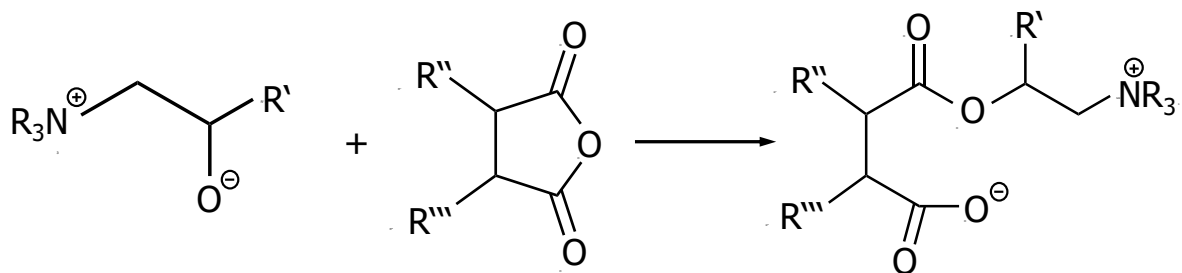


**Figure 11: formation of a carboxylate ion through the reaction of alkoxide**

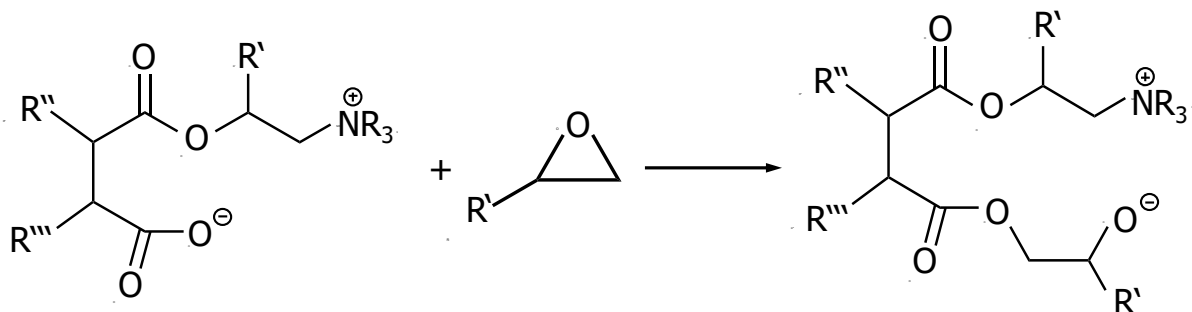


**Figure 12: carboxylate anion reacts with epoxy, leading to chain propagation**

## 2. Theory

---

Summing up the previously described mechanism, sources nowadays assume that the curing of epoxy resins with anhydrides, catalyzed by tertiary amines, advances as an alternating anionic ring opening copolymerization – a chain polymerization mechanism [25, 31].

As for side reactions, also homopolymerization of epoxy bearing molecules is taking place. It was mentioned previously that this is primarily the case if there is an excess of epoxy and elevated temperature.

Concerning termination, opinions and findings differ within the scientific community. At present, there is no concrete answer as to whether there is a specific termination step. Different possibilities have been proposed, e.g., the initiating tertiary amine staying covalently bound to the polymer, potentially enabling living polymerization, or the same tertiary amine is reconstituted [25, 32, 33].

In the course of the experimental work for this thesis, no external catalyst was used. However, the epoxy monomer used – *N,N*-diglycidyl-4-glycidyoxyaniline (DGOA), pictured in Figure 6 – features a tertiary amine moiety, and belongs to the group of amino-glycidyl epoxy resins. Scientific work has already been done on DGOA as well as on other members of this resin class to show that the tertiary amine group has the capability to catalyze the curing reaction between epoxy and anhydride groups. Polymers produced from anhydrides and similar epoxy monomers therefore follow the scheme of a base catalyzed anionic polymerization [26, 31, 34].

## 2.3 Interpenetrating Polymer Networks

In 1960, the first usage of the term “interpenetrating polymer network” (IPN) was reported in a paper by J. Millar [35], although they have been unknowingly produced for the first time as early as 1914. Polymeric materials are classified as IPNs when they comprise at least two polymer networks, which are not covalently connected with each other but entangled on molecular scales at least to some extent. Depending on the preparation route, IPNs can be divided into two subcategories: Sequential IPNs, where the components for the second network are dissolved within the first network and crosslinked after the first network is complete, and simultaneous IPNs, where both networks are formed at the same time with the monomers all mixed together beforehand. In this case, the chosen paths for polymerization must not interact with each other because otherwise, two (or more) different networks could not be formed concurrently. A combination of an ionic and a radical reaction mechanism is therefore a valid example for realizing simultaneous IPNs. Figure 13 is a depiction of these two routes for producing IPNs. Moreover, also the composition of an IPN can be used to differentiate types of IPNs. Usually, they consist of at least two crosslinked thermosetting networks, in semi-IPNs though one component is a thermoplastic polymer [36, 37].

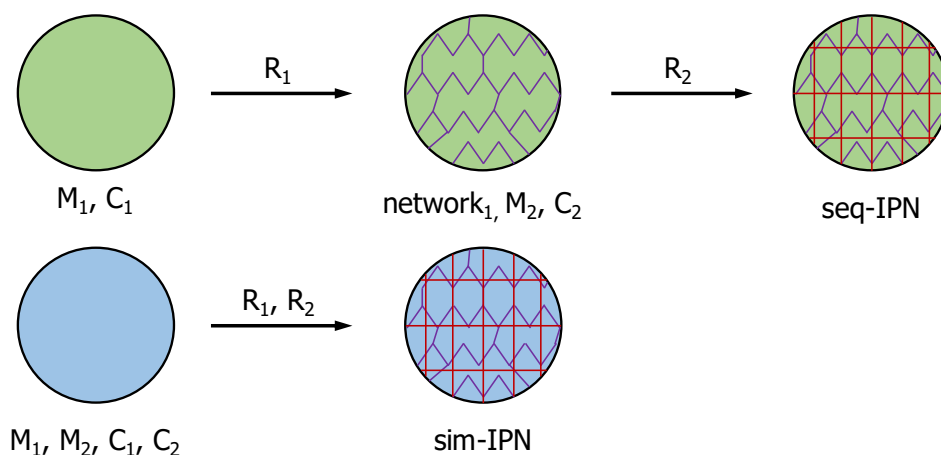


**Figure 13: schematic illustration of the difference between sequential IPNs (seq-IPN) and simultaneous IPN (sim-IPN), adapted from [38]. Abbreviations:  $M_1$  - monomer 1;  $C_1$  - crosslinker 1;  $R_1$  - reaction 1;  $M_2$  - monomer 2;  $C_2$  - crosslinker 2;  $R_2$  - reaction 2**

It should be noted that there is a significant difference between the “ideal” IPN and reality, as ideally, IPNs are completely homogenous at molecular scales. In practice, two polymeric materials with distinct properties are combined and enmeshed with each other. Although the individual networks have the thermodynamically determined desire to separate from each



## 2. Theory

---

other, molecular entanglement keeps them from doing so. Still, on nanoscale, phase separation phenomenon can be observed. Therefore, the composition of every small area within the entire material is different as the ratio of one polymer to the other varies throughout. As a result, the properties of (phase-separated) IPNs cannot be compared to those of random copolymers or even block copolymers. The interpenetrating realms, created through the enforced combination of two-network materials act as a distinction between IPNs and polymer blends. Altogether, it is very difficult to accurately define and identify an interpenetrating polymer network, as oftentimes the boundaries between similar material types are blurred [38, 39].

If the two (or more) networks in an interpenetrating system are – to a limited extent – connected covalently with each other, the resulting material is called “interconnected polymer network” (ICN) or also hybrid material. In Figure 14, the differences between IPNs, semi-IPNs and ICNs are illustrated. In order to achieve a hybrid network, a monomer which can partake in both polymerizations is necessary – such monomers are sometimes referred to as bridging agents. In the case of the present work, the anhydride monomer contains a C=C double bond in addition to the anhydride moiety. Therefore, it is able to participate in the free radical acrylate polymerization as well as in the epoxy curing. Lantean et al. experimented with bridging monomers that had an acrylate group as well as an epoxy group. They observed influences on conversion as well as crosslink density, as especially the acrylate network was subjected to more chain termination and therefore less crosslinks. As a consequence, properties such as damping behavior are affected as well [38, 40].

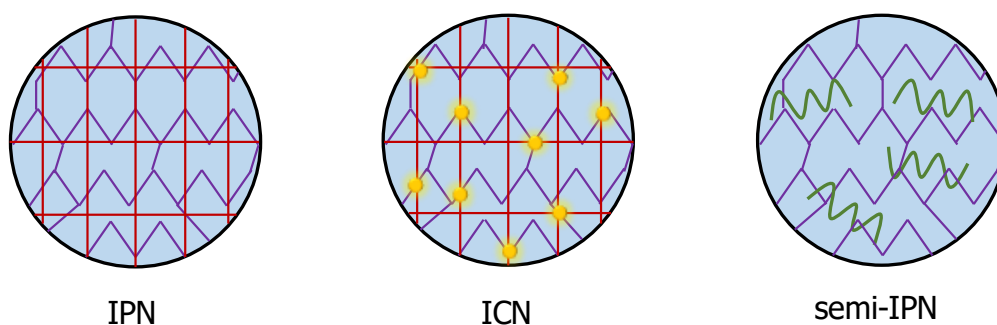


**Figure 14: comparison of the structures: IPN, ICN, semi-IPN, adapted from [38]**

Today, there are numerous different IPNs that have been investigated and produced. Double network hydrogels for example constitute one of the largest groups of IPNs. IPNs and related research are opening up numerous applications in various fields as new combinations of polymers bring new properties. On the one hand, increased mechanical properties are an attractive feature, i.e., in impact applications where good damping is a sought-after trait. Here,

## 2. Theory

---

especially latex-based IPNs find use. The medical field has a high interest in interpenetrating polymer network materials as well – a prominent example are soft contact lenses. Additionally, there are reports of IPN research for usage in dressing of burns, drug release systems, implants and many more [41].

Summarizing, IPNs are an extensive topic that is often difficult to outline due to the numerous overlaps with other polymer networks. Additionally, the networks formed and the dynamics involved are usually highly complex – even changes in the sequence of polymerization can lead to new material properties. Therefore, it is very challenging if not impossible to accurately predict the properties of an IPN or hybrid network beforehand [42].

### 2.3.1 Dual-Curing

One refers to “dual curing” to describe two distinct curing reactions being combined to produce a material comprising two polymer networks. As the previous chapter suggests, the result of dual curing is often an IPN, although also hybrid interconnected networks are possible. Dual curing is usually sequential but can also be simultaneous, although there is less room for influencing the consequential network structure with this approach. The sequential procedure, however, entails that a stable intermediate state can be reached after completion of the first curing step. It is important that during this transition state no chemical curing reactions take place until triggering the next reaction. Obviously, an intermediate product cannot be produced via the simultaneous route. There are two types of dual curing systems as far as the starting formulation is concerned: one-pot and two-pot systems – the latter being less flexible as curing starts with the combination of the two components. One-pot systems commonly consist of a mixture of liquid monomers – no solvents are needed, which is advantageous. It is essential that both curing mechanisms have different triggers, e.g., light and temperature and that the respective reactions are compatible without unwanted side-reactions in order to successfully realize sequential dual curing. Due to the nature of the sequential curing process, it is possible to modify the properties of immediate and final product through monomer ratio as well as curing duration and temperature. Dual curing is not only about influencing the resultant network but also about implementing the curing procedures technically. It is necessary to pay attention to the risk of exothermic curing reactions, as well as to undesirable temperature increases during curing or storage of the intermediate. The thermal discharge of lamps used for photo-induced curing for instance can lead to involuntary heating of the material. If the second curing step has a thermal trigger, these aspects are of particular importance [43, 44].

## 2. Theory

---

Acrylates have been involved in reactions with a variety of other molecules due to the reactivity of their double bond, e.g., thiol-ene reactions. Those reactions can be implemented in dual-cure systems through the use of different initiators [43]. Dual curing combinations of different reactions with the acrylate homopolymerization have been reported in the last years, such as thermally initiated cationic polymerization of epoxides with a photo-initiated radical polymerization of the acrylate. Systems like this are possible if the curing reactions proceed via different chemical reaction mechanisms that do not interfere with each other [42]. Park et al. also reported a dual cure system consisting of photochemically and thermally cured acrylates in combination with epoxides cured via an anionic route [45]. Besides merely irradiating samples with a lamp to implement photopolymerization, incorporating 3D-printing into a dual-curing process offers many possibilities. An ink that is processable through 3D-printing and subsequent thermal curing was presented by Kuang and coworkers. They used a triacrylate for photopolymerization (3D-printing) and thermally post-cured their sample through the contained epoxy-anhydride formulation. When tensile testing was performed before and after the thermal curing step, an increase in Young's modulus of up to 200 times could be achieved due to the formation of the epoxy network [46]. Another implementation of dual curing was introduced by Cazin et al. In their work, an epoxy-acrylate resin was subjected to dual wavelength 3D printing – the two different networks each responded to one illumination wavelength and proceeded independently. Spatiotemporal control of mechanical properties is an attractive advantage of this strategy [47]. These and similar approaches show, that dual curing is an important way to improve mechanical properties of thermosetting resins as well as enhance the opportunities that 3D-printing brings to the table [48]. A visual representation of a dual curing process is given in Figure 15.

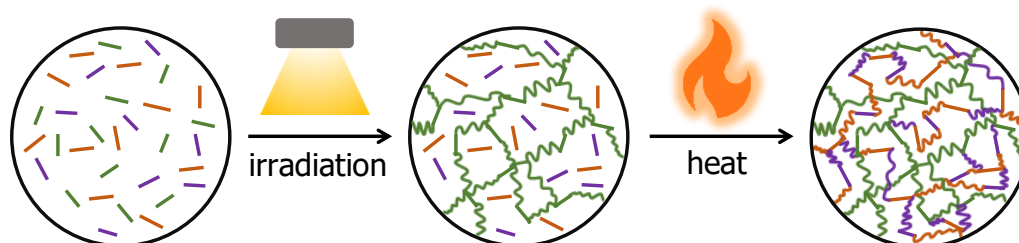


**Figure 15: exemplary dual curing process, adapted from [43]**

### 2.4 Vitrimers

Vitrimers are a relatively novel group of polymeric materials – they were first described in 2011 by Leibler et al. They descend from the closely crosslinked thermosets, which are insoluble and cannot be reprocessed or molten. Contrary to the properties of thermosetting polymers, thermoplastics consist of linear molecules that can be transferred into a flowing state by applying heat, making them processable through various techniques, such as extrusion or injection molding. However, thermosets entail indispensable advantages, especially mechanical and thermal properties, that make them a necessity in sectors such as aviation and building of wind turbines – specifically when processed into composites [49, 50].

Exchangeable covalent bonds enable crosslinked materials to get the best of both worlds: superior mechanical properties but also flexibility. Elevated temperatures are mostly used to prompt the bond exchange, although also other stimuli have been reported [51]. These polymers have been termed covalent adaptable networks (CANs) and can be allocated into two main groups: Associative CANs and dissociative CANs. Materials belonging to the first group are able to partake in bond exchange by creating a new crosslink at first and thereafter breaking up another bond. As a result, the average crosslink density within those networks stays constant. Dissociative CANs however display a different behavior, as here the crosslinking bonds are broken before new ones are formed. Consequently, at temperatures where the interchange reactions can proceed fast, the crosslink density declines fast, causing the material's viscosity to perform likewise. This trend in viscosity is reminiscent to that of thermoplastic polymers. When a CAN is subjected to an external stress, its response is dependent on the rate of the crosslink exchange reactions: If the interchange is slower than the period of external stress, the network's behavior resembles a common thermoset; if it is faster though, the behavior tends to be of a viscoelastic nature [50, 52]. In Figure 16 and Figure 17, the distinction between associative and dissociative networks is graphically illustrated.

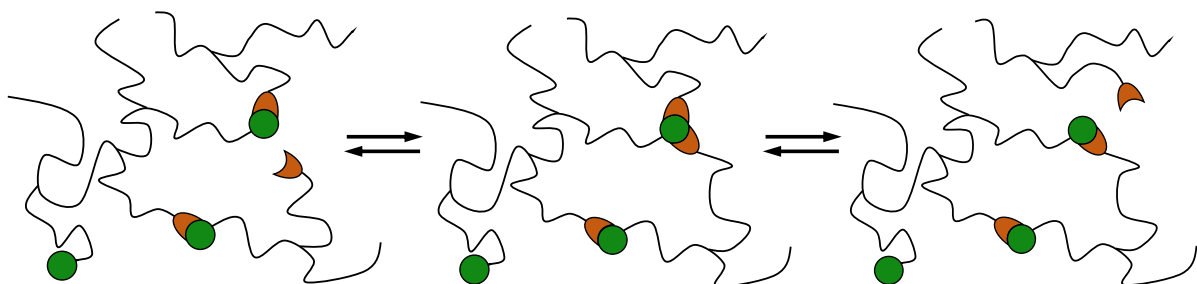


**Figure 16: schematic crosslink interchange of an associative network, adapted from [53]**

## 2. Theory

---

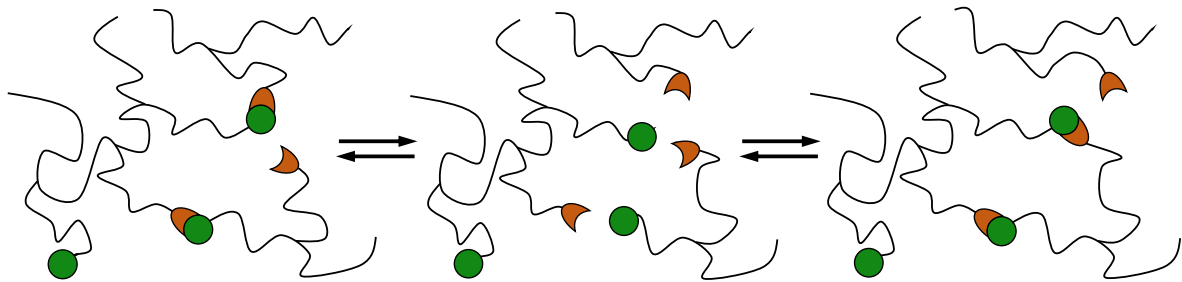


**Figure 17: schematic crosslink interchange in a dissociative CAN, adapted from [53]**

Through the combination of thermosets and the flexibility of interchangeable crosslinks, CANs facilitate possibilities such as self-healing, changes of shape, relaxation of inner stresses or recycling. As environmental consciousness has been on the rise in the last few years, these properties are highly utilitarian – self-healing enables repair processes and recycling makes it possible to sustainably reuse materials [50].

Vitrimers are part of the group of associative CANs, therefore they display a constant number of crosslinks. If vitrimers are subjected to rising temperatures, the rate of crosslink exchange rises as well. When the material's temperature is high enough, the dynamic reactions lead to a decrease in viscosity with increasing temperature. Obviously, also thermoplastic materials are subjected to a decrease in viscosity at elevated temperatures, but in this case, the underlying mechanism is an increase in the movement of polymer chains and disentanglement of the same. Additionally, also the courses of the decrease vary greatly. In thermoplastic polymers, the viscosity decreases abruptly, whereas vitrimers encounter a much more gradual decline. Accordingly, it is necessary to apply distinct mathematical descriptions to those phenomena [52, 53].

Inherently, most organic materials and therefore also thermoplastic polymers are so-called fragile glass formers. In this context, the term "fragile" refers to the abruptness of a change in material behavior in the proximity of glass transition. Hence, it can be deduced that for traditional (thermoplastic) polymers the viscosity rises significantly and steeply if the temperature is brought below  $T_g$ . Simultaneously occurs a hardening of the material – it transitions from its formerly rubbery state to a glassy shape. This process is usually called vitrification. For thermoplastics, the slope of the rise in viscosity is best described with the Williams-Landel-Ferry (WLF) law.

As previously mentioned, vitrimers experience a steadier viscosity decrease based on exchange reactions at elevated temperatures and their glass transition temperature is best described as a range. Resembling the behavior of silica – glass, in other words – they are characterized

## 2. Theory

using the Arrhenius law. Their similarity to vitreous silica in this aspect also coined the expression “vitrimers”. In order to provide an accurate description of the thermal properties of vitrimeric materials,  $T_g$  is not sufficient as they possess another transition temperature: the topology freezing temperature ( $T_v$ ). It was introduced by Leibler and his coworkers to mark the passage between viscoelastic liquid and elastic solid.  $T_g$  also exists in vitrimers, but – same as for thermoplastic polymers – refers to thermally initiated chain movement. For the purpose of expediency,  $T_v$  is defined as the temperature at which the vitrimeric material attains a viscosity of  $10^{12}$  Pa s [2, 49]. Figure 18 compares the progression of the viscosity curves for thermoplastics and vitrimers.

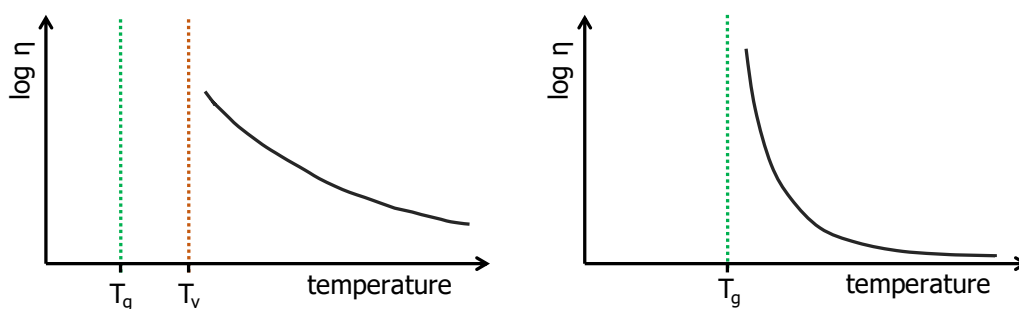


**Figure 18: left: Arrhenius dependent behavior of viscosity in proximity of  $T_v$  as with vitrimers; right: viscosity graph of a thermoplastic polymer above  $T_g$ ; figure adapted from [2]**

Summarizing, the main distinguishing features of vitrimers are thermally triggered exchange reactions between crosslinks of an otherwise thermoset-like network and the resulting viscosity behavior. As vitrimers are associative CANs, the crosslink density and therefore the stability of the network remains constant, leading to properties such as insolubility. From a chemical perspective, there are different approaches to achieve vitrimeric behavior [52]. Among mechanisms such as transamination reactions in vinylogous urethanes [54], transalkylation of triazolium salts [55] and others, transesterifications are widely spread. In a transesterification reaction, the reactants are hydroxyl moieties and carboxylic esters. During the equilibrium reaction, they are converted into new alcohol and new ester groups. As the transesterification is an associative reaction, there is an intermediate step where all reactants connect with each other transitionally before cleaving the former crosslinks, leaving only the new ones to remain. Prerequisite for a transesterification to actually take place – especially within a network – are adequate amounts of both carboxylic esters as well as hydroxyl groups [2]. Figure 19 illustrates a model transesterification reaction. Due to the wide range of monomers available, transesterification based vitrimers have been in the focus of research globally for the last

## 2. Theory

---

years [52]. The first vitrimers were made from epoxy-acid- and epoxy-anhydride-networks [49], since then also other networks have been used, such as thiol-ene for instance [56, 57].

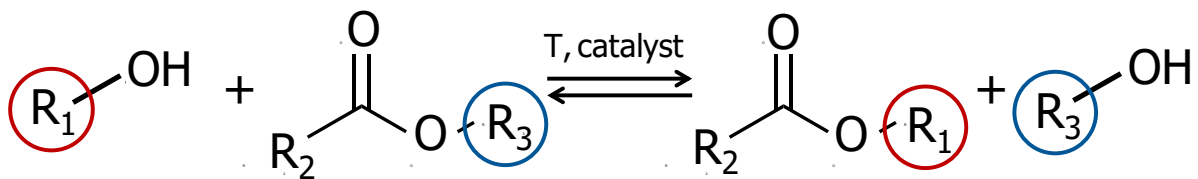


**Figure 19: schematic illustration of a transesterification reaction**

Beside a sufficient number of free hydroxyl- and ester moieties, also a suitable catalyst has to be introduced to achieve rapid exchange reactions above the network's  $T_v$ . A variety of substances has been used in this context – mainly inorganic salts or organic bases. Zinc acetylacetonate hydrate, an organometallic complex, found use in an acrylate-based system for 3D-printing [58] and the base 1,5,7-triazabicyclo[4.4.0]dec-5-ene (TBD) was implemented to catalyze transesterification in a thiol-ene system for nanoimprint lithography by Lyon et al [56] – to quote a few examples. As the rate of the crosslink exchange reactions is depending on the amount and nature of the catalyst, its deliberate selection is of particular importance [2].

Since the introduction of vitrimers there has been a considerable number of papers published about epoxy vitrimers [59]. Different transesterification catalysts were studied scientifically, such as  $\text{Zn}^{2+}$  [60], TBD or triphenylphosphine [2]. But those chemicals have some significant downsides, as they are often toxic and poorly soluble in monomer solutions. If too high amounts of catalysts are incorporated into the resin, mechanical properties might be influenced negatively if mixed insufficiently [61]. In 2019, a paper published by Williams et al. described the catalysis of transesterification reactions through covalently bonded tertiary amines. They produced a material with vitrimeric properties without the addition of a conventional catalyst. Starting with primary and secondary amines, which reacted with a surplus amount of epoxy monomers, molecules containing tertiary amines were obtained. Subsequently, these new epoxide molecules underwent curing with carboxylic acids – thus conveniently generating hydroxyl moieties able to partake in transesterification. Through stress relaxation experiments, the vitrimeric character of this material was proven [62]. More recently, Giebler and coworkers used a similar approach of using epoxy monomers containing tertiary amine moieties in the curing of epoxy-anhydride networks. They also were able to demonstrate that their material was indeed a vitrimer through stress relaxation experiments. Additionally, successful recycling in form of grinding and remolding the network was reported [34]. Concluding it can be

## 2. Theory

---

assumed that covalently bound tertiary amine groups are indeed able to not only catalyze curing of epoxy-anhydride systems but also transesterification. It should be noted that in addition to a suitable catalyst, a sufficient quantity of esters and hydroxyl moieties is crucial to observe transesterification. As during the polymerization of epoxy monomers with anhydrides usually primarily ester groups are formed, a possible solution to this problem could be reducing the epoxy/anhydride ratio (from the usual 1:1) to an abundance of epoxy monomers. However, this negatively affects the crosslink density and as a consequence also the mechanical properties. Nevertheless, Zhang et al. presented an approach to (biobased) epoxy-anhydride vitrimers, showing that within their system the networks made up from a 1:1 epoxy/anhydride ratio exhibit faster relaxation rates, higher  $T_g$  and better healing properties. Using a self-synthesized trifunctional epoxy monomer, they attributed those surprising results to a relatively low rubbery modulus enabling chain movement and an adequate number of hydroxyl bonds [63].

In general, thermosets are nearly impossible to recycle or repair, as their covalent networks cannot be broken physically, nor can they be dissolved. Obviously, this is detrimental to a sustainable utilization of resources, as thermoset waste usually has to be incinerated or end in landfilling. Additionally, the inability to be reprocessed is a serious economic disadvantage to thermoplastics. Due to the dynamic nature of vitrimers, they enable not only healing, but also recycling, reusing and welding [64, 65]. Different approaches have been investigated and demonstrated, for instance an ink for 3D-printing that is reusable several times without a significant loss in mechanical properties. This behavior is realized by dissolving the printed network at elevated temperatures [65]. Another path that has been explored effectively is remolding the vitrimer under heat and pressure after grinding it into small particles [34, 64].

### 2.5 3D-Printing

In recent years the terms “additive manufacturing” or “3D-printing” have become indispensable. Since the first introduction of additive manufacturing technologies (AMTs) in the 1980s, they have advanced considerably – in scientific as well as commercial regards. The underlying principle is that a digital model is transformed into a physical item on a very direct route – skipping steps such as process planning or the manufacturing of specific tools. Advantages such as high freedom in the design and construction of printed parts and great potential for tailoring and customization contribute to the large popularity of AMTs [1, 66]. 3D-



## 2. Theory

---

printing applications are researched widely – the fields of interest include shape memory polymers for soft robotics [67], drug release systems [68], biomedical devices and many others [69].

Slicing 3D models created digitally into layers with a set thickness makes these models processable for 3D printers. Although this basic approach is similar to all kinds of AMTs, they still have distinguishing features, such as the processable materials, the layer buildup and the connection of those layers to each other. AMTs include systems based on extrusion, material jetting processes, powder bed fusion systems and last but not least vat photopolymerization. Obviously, all these systems can be divided into subgroups again [66]. As the 3D-printing system used for the experimental work on this thesis was based on photopolymerization, the rest of this chapter is going to focus on 3D printing of photosensitive materials, specifically.

Most often, photoreactive materials for 3D-printing are processed either via stereolithography (SLA) or digital light processing (DLP). In contrast to extrusion-based techniques, the processed material is a liquid resin for these approaches, which needs light of a specific wavelength and minimum intensity to cure. Stereolithography on one hand works with a moveable laser, which follows a path illuminating the resin surface and thus curing each layer [65]. On the other hand, there is the DLP approach which in comparison brings much lower printing times, as a whole layer is cured at once. DLP relies on a so-called digital micro-mirror device developed by Dr. Larry Hornbeck at the company Texas Instruments in the 1980s and 90s. This small projector device consists of numerous tiny mirrors – each mirror is responsible for one pixel in the projected image [70]. In order to be able to cure materials using the projector and light source, a resin vat (also known as a bath) with a transparent bottom is placed above. The moveable platform where the printed part is built on is immersed into the filled vat from above, only leaving a narrow gap – equal to the previously set layer thickness – between the bottom of the bath and the platform. Subsequently, the resin is illuminated in the desired shape from below and cured in the process. Obviously, dependent on the geometry to be printed, each layer has its own pattern for illumination. Between every layer, the platform rises a small distance and then acquires its new position. Figure 20 shows the simplified DLP setup.

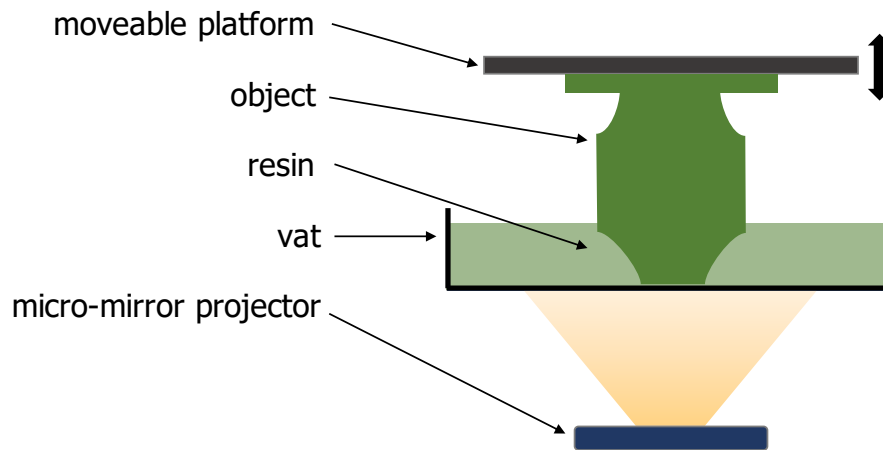


**Figure 20: simplified illustration of the DLP process, adapted from [57]**

Generally speaking, digital light processing offers many advantageous features, for example the low amount of resin required in the printing process, as there is only very little excess material needed. Oxygen inhibition was previously mentioned as a downside of acrylates – which are important monomers for photopolymerization based applications. Due to the fact that the illumination and therefore the curing do not take place under air but under the resin surface at the bottom of the bath, it does not pose a problem during DLP processing [1]. Another outstanding feature of DLP is the great surface quality, which is tunable through adapting the individual layer thickness, made possible by high resolutions. Especially contrasting extrusion-based approaches – which do usually not exhibit smooth surfaces – this is a notable plus. Flexibility in all aspects is also a beneficial trait of digital light processing, as light sources and their wavelengths, machine sizes and illumination patterns are changeable. As a result, a variety of materials as well as geometries can be subjected to the DLP process [66].

### 2.5.1 Possible Applications – Rapid Tooling

3D-printing has found a great variety of applications since its first invention. In the beginning, 3D-printed parts were mainly used as models to visualize new products during the designing process. Geometric flexibility and freedom in design are key advantages of additive manufacturing techniques – due to the layer-by-layer approach, it is possible to design a product according to the best functionality without affecting the manufacturing process. Additionally, the production of parts through AMTs can be realized very fast, as no previously

## 2. Theory

---

manufactured tools are necessary. Another benefit of AMTs is that they usually have rather low acquisition costs in comparison to other machines [66].

Markets and the economy today are fast paced, as new products are being developed daily. This brings a necessity for quick product development, high quality and a relatively low time to market in its wake. "Rapid manufacturing" is a term often mentioned in this context. It constitutes a combination of "rapid prototyping" (RP) and "rapid tooling" (RT), both pathways to improve the duration of product development. RP represents the production of functional prototypes and models that come straight from computer aided design (CAD) models. All commercially available AMTs are used in RP, as each has their own specific advantages. However, it is not possible to always rely on the use of models – prototypes also have to be produced conventionally, with the intended material and production process. If manufacturing techniques such as injection molding or extrusion are used, tooling is a particularly expensive part of the process. Here, RT comes into play – the direct usage of parts produced through additive manufacturing as tools, e.g., molds [3, 71].

There are different classifications for RT, although their boundaries are not set clearly and overlap partly. On the one hand side is soft tooling, comprising tools made out of polymeric materials mostly and tools that do not survive more than a few (or sometimes even one) cycles. Hard tooling on the other hand side usually involves tools and molds made from durable and tough materials such as tooling steel, being usable for mass production as well. Another differentiation is made between direct and indirect tooling. Whereas an intermediate part is necessary for indirect tooling in order to manufacture a mold and there is only one manufacturing step in direct tooling. Various materials have been used in direct tooling, such as ceramics or metal, but also epoxy based resins. In order to use polymeric materials, e.g., epoxy resins in RT, the processing temperatures of the handled materials have to be rather low, otherwise thermal impairment of the molds is the result. Soft direct tooling with epoxy resins is for instance used to produce molds for injection molding – plastic parts manufactured with these molds have high exactitude. Due to the rather moderate mechanical properties of the printable resins, the tools are likely to be corrupted during injection molding [3, 72].

Micro injection molding in particular is a potential field of interest for the utilization of RT – even more so for low numbered product series. Applications like these are for example found in the medical area. Mau and coworkers demonstrated micro injection molding of implants using a mold manufactured through DLP 3D printing of acrylate-based resin [73].

## 2. Theory

---

In summary, rapid tooling can be applied during the product development process, saving high costs for expensive tooling and great amounts of time. Less errors are prone to occur due to the immediate use of the CAD model when manufacturing the tool instead of interim steps. Additive manufacturing enables the ideal positioning of cooling channels in tools. However, there are still some disadvantages to RT – durability of the molds is an obvious downside. Shrinkage of the tools, especially when using polymeric materials, also has to be included into the construction process. Additionally, the surface quality of parts made from RT-molds is often inferior to that of conventionally manufactured ones. Last but not least, the range of materials being able to be processed through AMTs for RT has to be extended in the future [74].

## 3 Experimental

### 3.1 Chemicals

In the following table the chemicals used are listed.

**Table 1: used chemicals**

<b>chemical</b>	<b>abbreviation</b>	<b>manufacturer</b>
glycerol 1,3-diglycerolate diacrylate	GDGDA	Sigma-Aldrich
<i>N,N</i> -diglycidyl-4-glycidyoxyaniline	DGOA	Sigma-Aldrich
methyl-5-norbornene-2,3-dicarboxylic anhydride	MNA	Sigma-Aldrich
bisphenol-A-diglycidyl-ether	DGEBA	Sigma-Aldrich
ethyl(2,4,6-trimethylbenzoyl)phenylphosphinate	TPO-L	IGM resins
dichloromethane	DCM	VWR chemicals

### 3. Experimental

---

## 3.2 Devices

Table 2 lists all devices that were used during the experimental work on this thesis.

**Table 2: instruments used**

<b>instrument</b>	<b>manufacturer</b>	<b>model</b>
FTIR spectrometer	Bruker	Vertex 70
DSC device	Perkin Elmer	DSC 8000
Rheometer for viscosity	Anton Paar	MCR 102
Rheometer for SR	Anton Paar	Physica MCR 501
3D printer	Anycubic	Photon Mono
TGA device	Mettler Toledo	TGA/DSC thermogravimetric analyzer
UV-oven	formlabs	Form Cure
oven	Heraeus	T5042
tensile testing machine	ZwickRoell	Z1.0
vortex mixer	StateMix	VM-200
DMA device	Mettler Toledo	DMA SDTA 861e
curing lamp	Opsytec Dr. Gröbel	LEDControl 5S
spin-coater	Electronic Micro Systems Ltd	Spin Coater Model 4000

## 3.3 Preparation of the Resins

First, the acrylate GDGDA and the epoxy containing reagents DGOA or DGEBA were weighed in and mixed together homogenously at room temperature using the vortex mixer. After that, the anhydride MNA and the photo-initiator TPO-L were added, and the resin was again homogenized by the vortex mixer.

Table 3 lists all resins that were prepared and their respective compounds with their molar/weight percentage. Resin Ref-100:0 is a reference formulation that only contains

### 3. Experimental

---

GDGDA and photo-initiator, whereas Ref-50:50 and Ref-30:70 contain DGEBA instead of DGOA as a different epoxy reagent. It should be noted that "rest" in the table refers to the added contents of epoxy and anhydride. All formulations were calculated in a way so that the ratio between anhydride groups and epoxy groups is always 1:2 – as one cyclic anhydride is able to react with two epoxy groups.

**Table 3: resin formulations under investigation**

<b>resin name</b>	<b>ratio acrylate : rest</b>	<b>GDGDA mol%</b>	<b>DGOA mol%</b>	<b>DGEBA mol%</b>	<b>MNA mol%</b>	<b>TPO-L wt%</b>
R-50:50	50:50	50	20	0	30	2
R-40:60	40:60	40	24	0	36	2
R-30:70	30:70	30	28	0	42	2
R-20:80	20:80	20	32	0	48	2
Ref-100:0	100:0	100	0	0	0	2
Ref-50:50	50:50	50	0	25	25	2
Ref-30:70	30:70	30	0	35	35	2

### 3.4 3D-Printing and Thermal Curing

3D-printing was used to produce specimens for FTIR measurements, stress relaxation measurements, swelling tests, dynamic mechanical analysis, tensile testing and thermogravimetric analysis. All printing experiments were carried out using an Anycubic Photon Mono printer. The resins were produced immediately before pouring them into the vat of the printer. Illumination settings for the printer were selected based on an experimental approach for each resin formulation. All respective printing times are listed in Table 4. Rising speed and retract speed were both chosen to be 3 mm/s. Subsequently, the printed piece was rinsed with isopropanol to get rid of redundant uncured resin and heated up to 60 °C for 10 min while still on the platform, to facilitate removing it from said platform.

All 3D-printed pieces were subjected to the same post-curing procedure, which consisted of two separate steps. The first step entailed 20 min at 80 °C and constant UV-irradiation with

### 3. Experimental

---

405 nm. After that, the samples were put in an oven for purely thermal curing for 40 min at 150 °C.

The intensity of the printer used amounted to 4.42 mW/cm<sup>2</sup> and the intensity of the UV-curing oven was measured to be 9.96 mW/cm<sup>2</sup>.

**Table 4: printing settings**

resin name	exposure time (bottom layer) [s]	exposure time (normal layer) [s]
R-50:50	120	52
R-40:60	120	65
R-30:70	150	80
R-20:80	180	120
Ref-100:0	60	25
Ref-50:50	100	50
Ref-30:70	110	50

### 3.5 FTIR-Measurements

To analyze the curing behavior, FTIR-measurements were carried out. Measurements were performed in transmittance mode over a wavenumber range of 4000-650 cm<sup>-1</sup>. All spectra were accumulated from 16 scans at a resolution of 4 cm<sup>-1</sup>. The conversion of the functional groups was calculated with OPUS software by integration of the characteristic acrylate IR absorption band at 1636 cm<sup>-1</sup> and the absorption bands of the epoxy groups at 912. The C-H absorption band at 2900 cm<sup>-1</sup> and the C=O absorption band at 1730 cm<sup>-1</sup> were used as reference peaks. The overall conversion (*C*) of the curing reaction was obtained by the following equation,

$$C = 100 - \left( \frac{A_{peak}}{A_0} * \frac{A_{Ref,0}}{A_{Ref}} * 100 \right)$$

in which  $A_{peak}$  corresponds to the absorption area of the observed band of the cured sample and  $A_{Ref}$  to its reference peak.  $A_0$  and  $A_{Ref,0}$  correspond to the absorption areas of the respective peaks of the uncured sample.



### 3. Experimental

---

For sample preparation, 1  $\mu\text{L}$  of the respective resin was spin-cast on a Si wafer without solvent at a speed of 3000 rounds /min for 30 s. The spin-coater used was manufactured by Electronic Micro Systems Ltd. Visible light irradiation was carried out with a LED 405 nm curing lamp (intensity: 34.78  $\text{mW}/\text{cm}^2$ ) (Opsytec Dr. Gröbel) at a distance of 4 cm under nitrogen atmosphere and FTIR measurements were performed every few seconds. After photocuring, a 20 min curing step in the formlabs UV-cure oven at 80  $^{\circ}\text{C}$  – with FTIR-measurements every 5 min – was conducted. Lastly, 40 min of only-thermal curing at 150  $^{\circ}\text{C}$  was performed to mimic the post-curing procedure of the printed samples.

### 3.6 Dynamic Mechanical Analysis

In order to determine the  $T_g$  of the cured resins, dynamic mechanical analysis (DMA) was performed on a Mettler Toledo DMA SDTA 861e. The specimens were prepared through 3D-printing with a length of 30 mm, a width of 4 mm and a thickness of 1.5 mm and underwent post-curing according to chapter 3.4. DMA testing took place under a nitrogen atmosphere in a displacement-controlled mode. Temperature was ramped at a pace of 2 K/min starting at 30  $^{\circ}\text{C}$  and ending at 250  $^{\circ}\text{C}$ . The frequency applied amounted to 1 Hz with a maximum amplitude of 10  $\mu\text{m}$ .

### 3.7 Differential Scanning Calorimetry

Differential scanning calorimetry (DSC) measurements were used to analyze the curing temperature of the epoxy on the one hand and the curing time at 150  $^{\circ}\text{C}$  on the other hand. For the latter, isothermal measurements were done at a temperature of 150  $^{\circ}\text{C}$  and the heat flow was recorded over time. The samples for DSC measurements were prepared by curing a drop of approximately 10 mg resin in the crucible with the 405 nm wavelength curing lamp. In order to determine the curing temperature peak, a program with 6 steps was run for each sample. First, an isothermal step at -30  $^{\circ}\text{C}$  for 5 min was performed, followed by a heating ramp to 220  $^{\circ}\text{C}$  with a heating rate of 20 K/min. After reaching 220  $^{\circ}\text{C}$ , the temperature was kept constant for 1 minute, before cooling to -30  $^{\circ}\text{C}$  with a cooling rate of 20 K/min and another 3 min isothermal at said temperature. In total, two heating runs were carried out for each sample. The heat flow over temperature was recorded for each cycle. For all DSC measurements a constant nitrogen flow of 20 mL/min was applied.

## 3.8 Stress Relaxation

Stress relaxation measurements were performed on a Physica MCR 501 rheometer from the manufacturer Anton Paar to monitor the bond exchange reactions. Torsion mode with corresponding equipment – a rectangular torsion fixture – was used for the specimens with the dimensions 20 x 4 x 1 mm. Measurements were taken at a temperature of 200 °C (and for the Arrhenius plot at 210, 220 and 230 °C). In the beginning, a set normal force of -0.05 N, which stayed constant during the complete run, was applied to the sample. The rectangular sample was subjected to the measurement temperature to equilibrate for a designated time, before applying a rotational deflection of 1 %. As an output, the decrease of the relaxation modulus was recorded over time.

## 3.9 Swelling Measurements

Swelling measurements were performed on printed specimens before and after thermal post-curing. After weighing 3 specimens per resin, the samples were put into 5 mL of dichloromethane for 24 h. Subsequently, the samples were dabbed dry with tissue paper for 10 s and put into an oven at 60 °C for 48 h. Following that step, the weight of the dry specimens was noted again. The measured values were averaged and the alterations in weight were calculated as percentages using the following formula:

$$wt\% = \frac{100}{w_0} * w$$

Here,  $wt\%$  stands for the percentage of original weight,  $w_0$  is equal to the original weight and  $w$  is the weight after drying the samples.

## 3.10 Tensile Testing

From the resins R-30:70, Ref-100:0 and Ref-30:70, samples for tensile testing were produced through 3D-printing according to chapter 3.4. The dimensions of the specimens correspond with the sample type 5B (12 x 2 x 1 mm) from DIN EN ISO 527-2. Experiments were done on a Z1.0 tensile testing machine from the manufacturer ZwickRoell. Clamping length was set to 20 mm. Determining the Young's modulus was done according to the standard; at a velocity of 1 mm/min between a strain of 0.05-0.25 %. Thereafter, speed was changed to 5 mm/min.

## 3.11 Thermogravimetric Analysis

3D-printed specimens were used to perform thermogravimetric analysis (TGA). Analysis took place in a TGA/DSC thermogravimetric analyzer (Mettler Toledo) under nitrogen atmosphere with a heating rate of 10 K/min from 23 °C to 900 °C. At 600 °C a switch happened from nitrogen atmosphere to oxygen and at 900 °C the measurement was stopped and the resulting mass reduction over temperature was graphed.

## 4 Results and Discussion

In the course of this thesis, selected resin formulations were developed and compared, aiming at vitrimeric resins with a comparably high  $T_g$  and decent printability. Therefore, the contents of the components were varied – especially the ratio of acrylate to the other two crosslinking components: epoxy and anhydride. In the four resins R-50:50, R-40:60, R-20:80, and R-30:70 the acrylate : epoxy-anhydride ratios were changed gradually from 50:50 to 20:80. Ref-100:0 acts as a reference formulation containing only acrylate and photo-initiator. Ref-50:50 is another reference resin, but with DGEBA instead of DGOA, as DGEBA contains no tertiary amine groups and should therefore not be able to catalyze transesterification. In Ref-50:50, the acrylate : epoxy-anhydride ratio is 50:50. For tensile testing, another resin was introduced – Ref-30:70 – which also contains DGEBA in place of DGOA but here the ratio is 30:70.

An important aspect to be considered is that the molecular structure and functionality of DGEBA and DGOA are not comparable. While DGOA contains three epoxy groups, DGEBA only contains two. This leads to a difference in network structure, as the crosslink density is probably lower in the DGEBA containing resins than in the others. Furthermore, the absence of tertiary amines in DGEBA does not only influence the potential transesterification reactions but also the curing reaction between epoxide and anhydride, as it is also catalyzed through amines. The hydroxyl moieties provided by the acrylate are also able to catalyze the epoxy-anhydride curing, but nevertheless the reaction potentially proceeds at a different rate than the amine catalyzed curing.

It should be noted that the contents of epoxy and anhydride were calculated in such a way that the number of epoxy groups equals half the number of anhydride groups – as one anhydride is able to react with two epoxy groups.

### 4.1 Curing of the Resins

The curing of the resins investigated in this work was split into two separate steps – photocuring and thermal post-curing.

#### 4.1.1 Differential Scanning Calorimetry

In order to gain insight into the thermal curing kinetics of the epoxy-anhydride network, DSC measurements were performed on R-50:50 and R-30:70. Figure 21 and Figure 22 picture the graphs derived from the two heat runs performed during the first experiment. In both runs, the sample was heated up from -30 °C to 220 °C with a heating rate of 20 K/min. In the first run, the epoxy-anhydride curing reaction can be observed for both resins, which resulted in a sharp peak (see Figure 21 and Figure 22). Since the curing reaction is exothermic, the resulting enthalpy of reaction  $\Delta H$  ("Delta H" in the graph) has a negative value and amounted to -78.7 J/g for R-50:50 and to -132.8 J/g for R-30:70. Due to the lower amount of epoxy-anhydride components in the first formulation, the enthalpy of reaction assumes a lower absolute value here than in R-30:70.

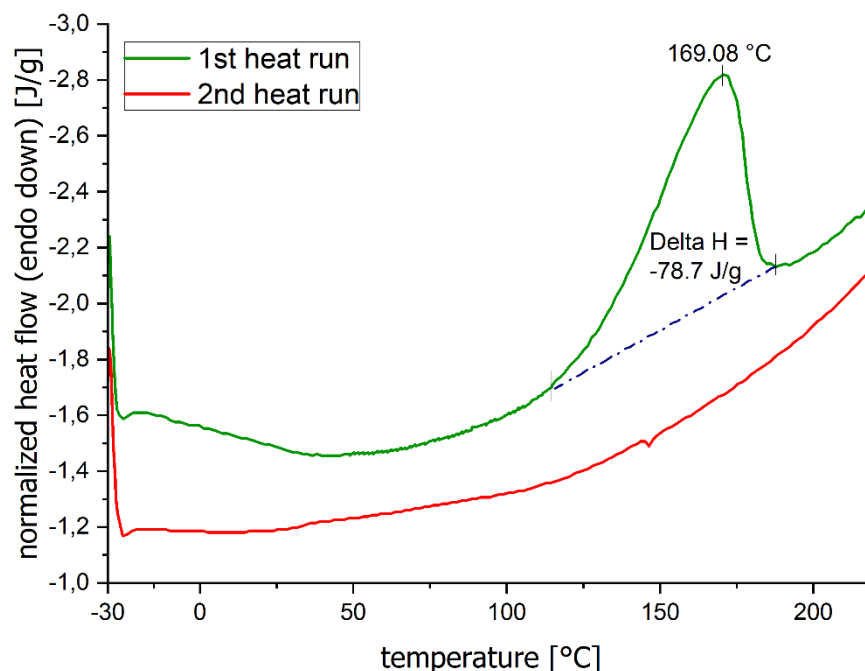


**Figure 21: DSC curves of the first and second heat run of R-50:50**

#### 4. Results and Discussion

In the second heat run, no peak is visible, which indicates that the curing reaction has been completed during the first run. It is not possible to observe a glass transition in the DSC curves. The onset temperature of the reaction was calculated to be 130 °C in R-50:50 and 131 °C in R-30:70; the peak temperatures amount to 169.1 °C and 170.4 °C, respectively. At the peak temperature, the material experiences the highest rate of reaction. These temperatures were taken into consideration when choosing the curing temperature of 150 °C – it had to surpass 131 °C for a reaction to take place. It was chosen to stay below the peak temperature of approximately 170 °C because of several reasons. Due to the exothermicity of the epoxy-anhydride curing reaction, additional heat is produced which can further increase the actual curing temperature. This can even lead to degradation if temperatures are too high. Commonly, lower reaction temperatures are chosen as a result – especially for larger parts [23]. For some epoxy-anhydride systems it has also been reported that the  $T_g$  can be influenced by the isothermal curing temperature, as the curing mechanism tends to favor different products if the curing temperature is too high. Additionally, higher curing temperatures in epoxy-anhydride systems lead to higher volumetric shrinkage – resulting in residual stress [75]. Those reports were considered when choosing the curing temperature in the second thermal treatment.

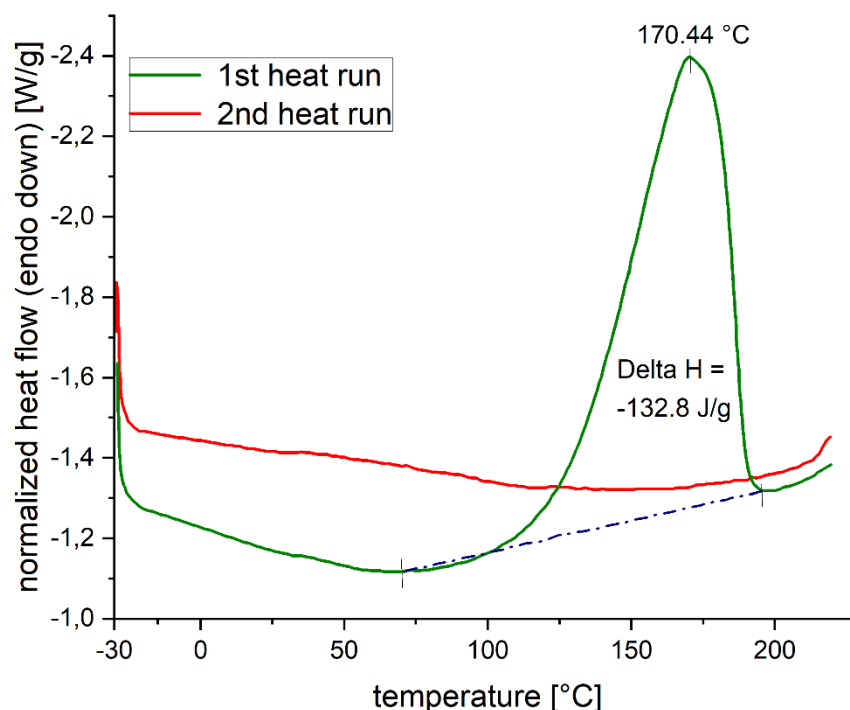


**Figure 22: DSC curves of the first and second heat run of R-30:70**

#### 4. Results and Discussion

---

Additionally, an isothermal DSC experiment was performed on R-30:70 resin at 150 °C. Figure 23 shows the resulting heat flow over time. The first 0.87 min were cut out of the plot due to settling time during heating. At the beginning, the reaction proceeded quite fast, as shown by the steep descent of the curve. After 2 min of curing, the reaction slows down and remains nearly constant for the next 5 minutes. After 7 minutes, the curing reaction is nearly completed – at 8 min, no changes in the normalized heat flow can be observed.

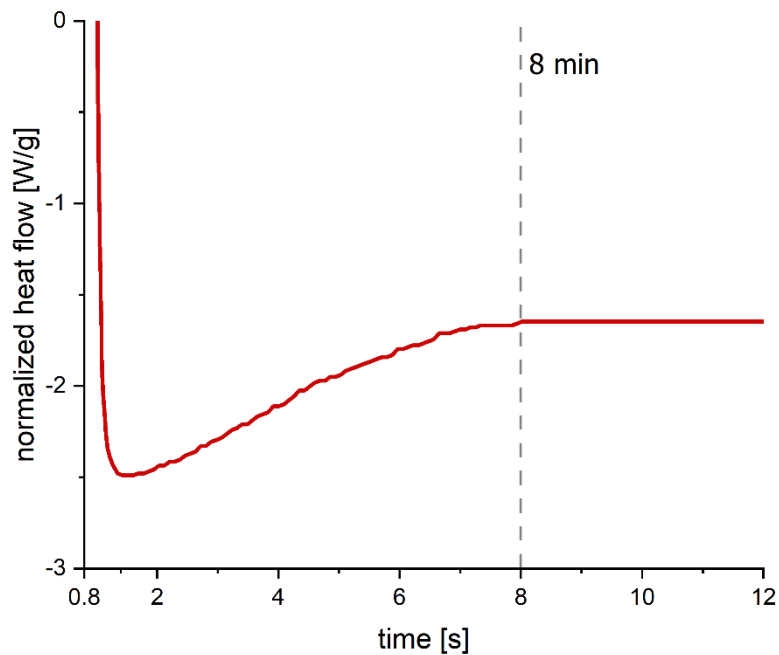


**Figure 23: isothermal curing of R-30:70 (30:70) at 150 °C**

Because it is observed that the curing reaction proceeds quickly at a curing temperature of 150 °C, it was concluded that it is a suitable temperature for curing. Therefore, 150 °C are chosen as the curing temperature in all following experiments.

### 4.1.2 Fourier-Transform Infrared Spectroscopy

Through FTIR measurements, the conversions of different functional groups were determined and plotted versus light/temperature exposure time. The functional groups, that were analyzed were the epoxy peak at  $912\text{ cm}^{-1}$  and the acrylate peak at  $1635\text{ cm}^{-1}$ . For the photocuring reaction, the C=O peak at  $1730\text{ cm}^{-1}$  was used as a reference peak and during thermal curing, the C-H peak at approximately  $2900\text{ cm}^{-1}$  served as a reference peak.

In Figure 24, the conversion of the acrylate peak at a wave number of  $1635\text{ cm}^{-1}$  is plotted against illumination time. In the beginning of illumination, all resins experience a steep ascent in curing rate within a matter of seconds. As soon as approximately 100 s of light exposure are reached, the curing speed slows down. At this point, the conversion of the acrylate groups is already fairly close to their final conversion at 300 s – which is a common occurrence in the radical polymerization of acrylates [76]. It is noticeable, that the different resins do not reach the same percentage of acrylate conversion. Additionally, it is possible to identify a trend regarding the acrylate content in the resins and the curing kinetics. R-20:80 – with an acrylate content of 20 mol% shows the highest final conversion, followed by the resin with 30 mol% acrylates. The two formulations containing 40 and 50 mol% of acrylate monomers respectively reach a very similar level of conversion, which lies significantly lower than the levels of R-30:70 and R-20:80. However, a different behavior was expected – literature suggested that curing rates rise with rising acrylate content in the resin [77].

A possible explanation for this unexpected behavior are differences in coating thickness. Ref-100:0 showed lower thickness of the layer cured in this experiment than the other formulations – especially R-30:70 and R-20:80.

Another reason could be that the network is far more mobile in the resins containing less acrylate monomers – there are considerably more unreacted molecules present due to the higher amount of epoxy and anhydride monomers. These unreacted molecules are responsible for maintaining network mobility – therefore the unreacted acrylate monomers are able to diffuse and can partake in the curing reaction. As there are less epoxy and anhydride molecules available in R-50:50 and R-40:60, the network is less mobile, which leads to lower conversions, as acrylate monomers can be trapped and are not able to diffuse freely.



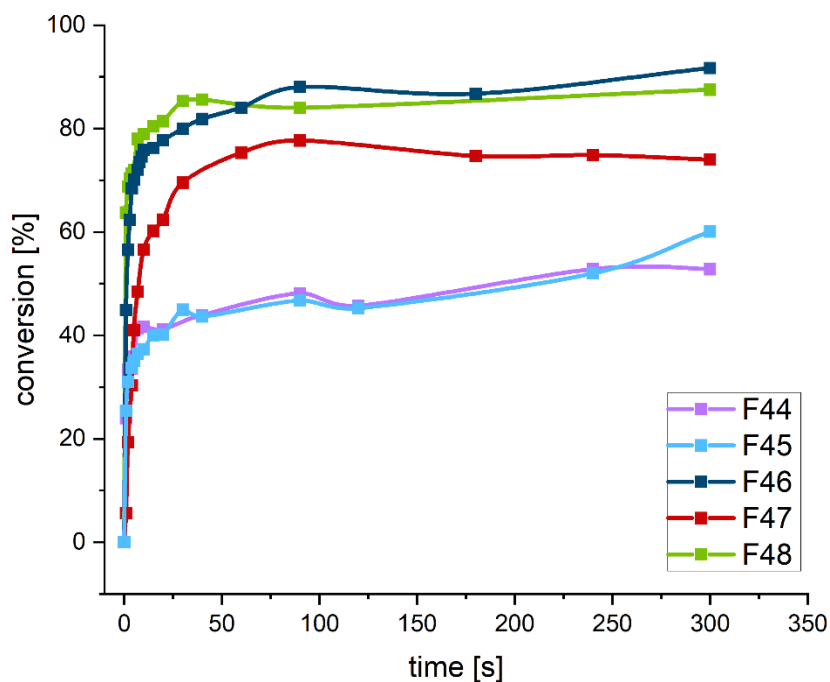


**Figure 24: Conversion of the acrylate band at  $1635\text{ cm}^{-1}$  plotted against curing time.**

Figure 25 shows the conversion of the epoxy C-O peak at the wave number of  $912\text{ cm}^{-1}$  during thermal treatment after illumination was finished. The first 20 min of curing are at a temperature of  $80\text{ }^{\circ}\text{C}$  followed by another 40 min at  $150\text{ }^{\circ}\text{C}$ . It is noticeable very clearly, that the reaction rate is highest in the beginning of the curing process. After the 5 min mark, the networks proceed with a mostly constant curing rate until the temperature switch happens at 20 min. The graph illustrates that the curing rate experiences a sudden increase in accordance with the temperature change. After the curing procedure, the final conversion is approximately 90 % for all networks except for R-40:60 and R-20:80 – their final conversions are above 80 %.

## 4. Results and Discussion

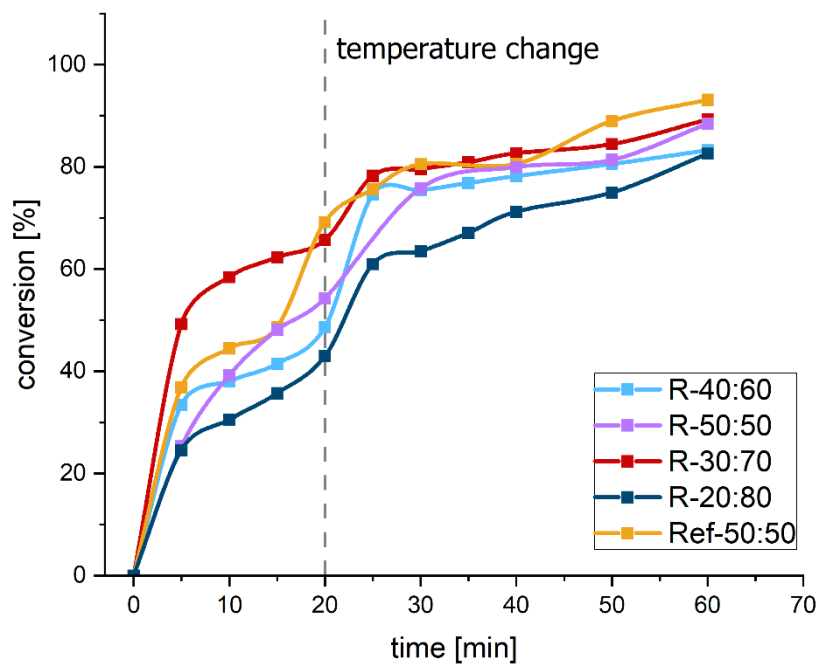
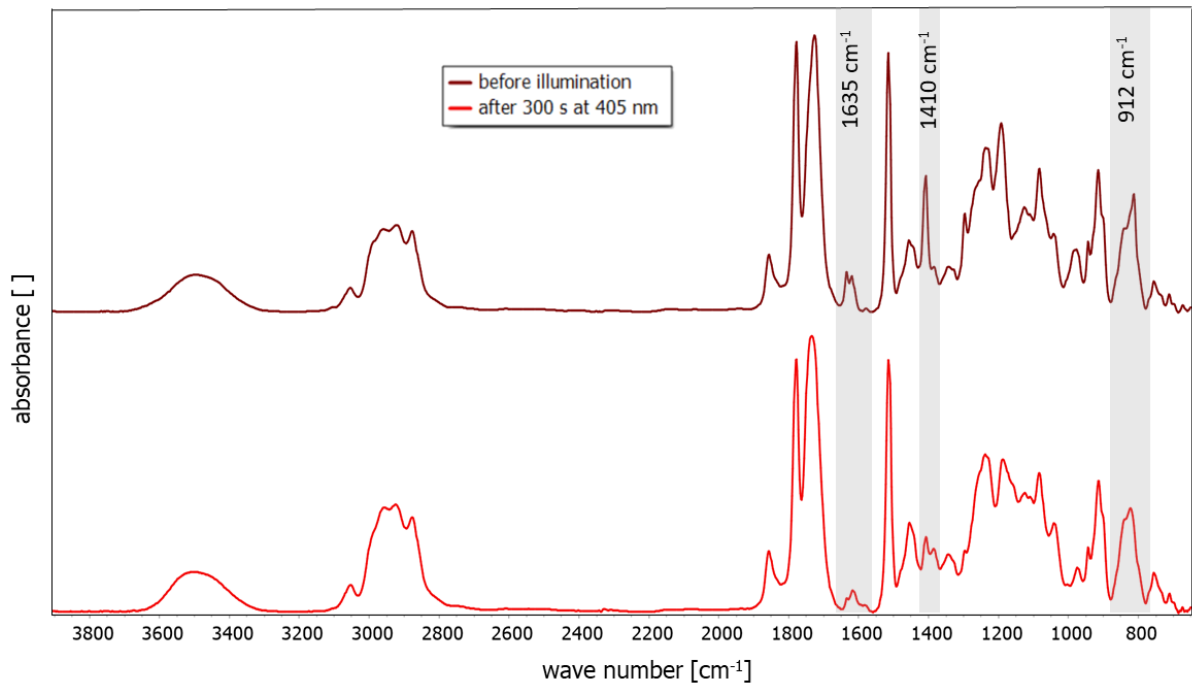


**Figure 25: Conversion of the epoxy band at  $912\text{ cm}^{-1}$  plotted against curing time. After 20 min, the curing temperature switches from  $80\text{ }^{\circ}\text{C}$  to  $150\text{ }^{\circ}\text{C}$ .**

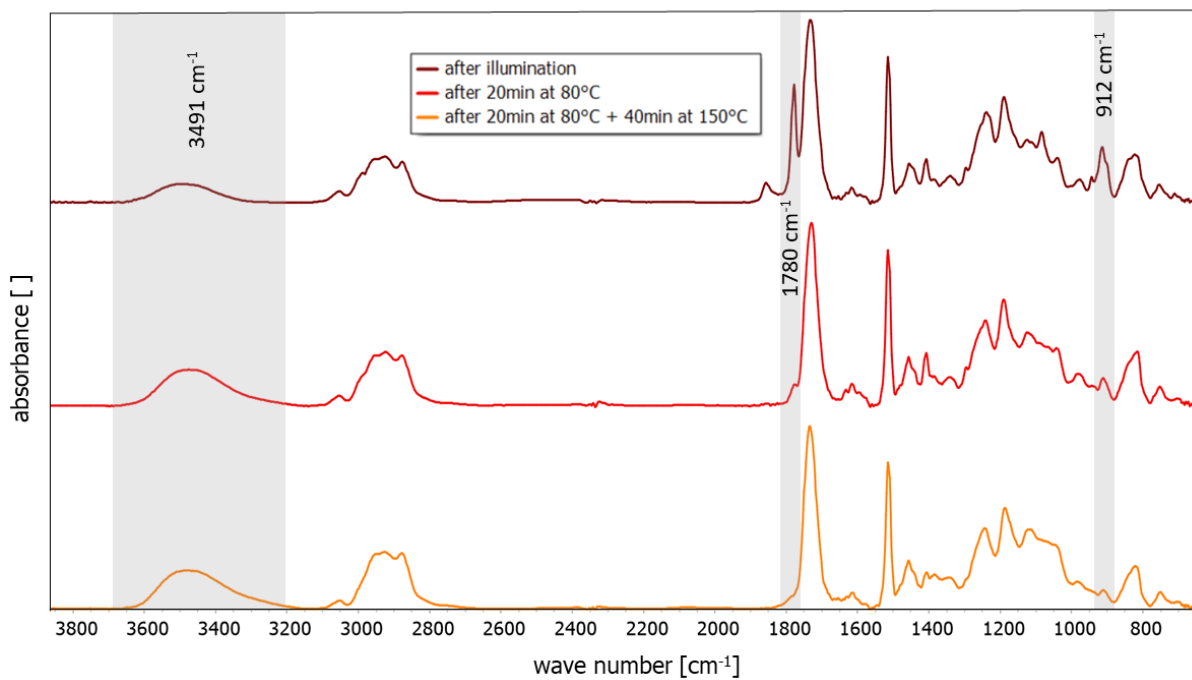
FTIR spectra recorded prior to and after illumination are compared for the resin R-30:70 in Figure 26. The two acrylate bands at  $1635\text{ cm}^{-1}$  and  $1410\text{ cm}^{-1}$  are labelled as well as the epoxy peak at  $910\text{ cm}^{-1}$ . It is clearly visible that the intensity of the two acrylate peaks decreases drastically during the illumination time which indicates a photopolymerization is occurring. As expected, the epoxy peak remains largely unchanged as it does not participate in the photoinduced curing reaction.

Figure 27 shows the spectra for the thermal curing reaction of R-30-70. In this illustration, the epoxy peak at  $912\text{ cm}^{-1}$ , the anhydride  $\text{C}=\text{O}$  peak at  $1780\text{ cm}^{-1}$ , and the peak of the OH-groups at  $3491\text{ cm}^{-1}$  are marked. The spectra show the state of the network after illumination, after 20 min of curing in the UV-oven at  $80\text{ }^{\circ}\text{C}$ , and after 40 min of curing time at  $150\text{ }^{\circ}\text{C}$  from top to bottom. Over the course of the thermal curing reaction, one can observe the disappearance of the epoxy and the anhydride peak. This indicates that the thermal curing reaction is proceeding. Additionally, the OH-peak shows an increase in height based on the formation of OH-groups during the epoxy-anhydride reaction. These hydroxyl moieties can be utilized during a potential transesterification reaction.

## 4. Results and Discussion



**Figure 26: FTIR spectra recorded before and after illumination for 300 s at 405 nm for the resin formulation R-30:70**



**Figure 27: FTIR spectra recorded after illumination for 300 s at 405 nm and after each thermal curing step for the resin formulation R-30:70**

#### 4. Results and Discussion

---

It is important to mention that in the case of the dual cured resins that were analyzed therein the acrylate conversion does not necessarily correlate with printability. This is especially the case for the resin R-20:80, which has an acrylate content of 20 mol%. Even though the conversion of the acrylate group is high – as Figure 24 shows – R-20:80 suffers from poor printability. The low amount of acrylates in the formulation is not able to build a network with adequate stability and quality that is able to fully contain the unreacted epoxy and anhydride monomers. Printed parts from R-20:80 exhibit a porous structure and incomplete shape retention. Those features cannot be compensated through thermal treatment and the curing of the second network. As a result, R-20:80 was not deemed to be a candidate for the possible application in additive manufacturing.

Generally speaking, the printing parameters were determined prior to specimen production. Bottom layer exposure times are vital for the adhesion between platform and printed piece. By gradually raising the illumination time of each resin until satisfactory adhesion is achieved, the exposure times for the bottom layer were determined. Table 4 shows that the resins with lower acrylate content need more illumination time to produce an adequate bottom layer. The higher amount of epoxy and anhydride components present hinders the adhesion as they remain unpolymerized until thermal curing. In order to set the curing times for normal layers – which are responsible for interlayer adhesion – the illumination times for the bottom layers were used as a reference. Starting from the value of the bottom layer illumination time, exposure time was decreased gradually as much as possible while maintaining printability. Rising speed and retract speed were set following prior experience – higher speeds were not possible, as the adhesion between bottom layer of the printed piece and platform was not strong enough to withstand a stronger pull. Through these tests, printing parameters were set that constitute a compromise between maximizing printing quality and minimizing printing time.

The parameters listed in Table 4 were then used to produce samples for DMA, stress relaxation, swelling experiments and tensile testing.

### 4.2 Thermal Properties

#### 4.2.1 TGA Measurements

In order to ascertain the temperature dependent degradation behavior of selected formulations, TGA measurements were performed. The knowledge of the degradation temperature was also necessary for further stress relaxation measurements to ensure that they can proceed within a temperature range where no thermal degradation is present. The two reference formulations Ref-100:0 (consisting of a solely acrylate-based network) and Ref-50:50 (using DGEBA instead of DGOA as the epoxy component) underwent TGA measurements as well as R-50:50 and R-20:80 – with an acrylate content of 50 mol% and 20 mol%, respectively. This selection of samples is representative of the other resins analyzed in this thesis. Measurements were done under a nitrogen atmosphere until a temperature of 600 °C was reached, then a switch to oxygen was made.

As is apparent from Figure 28, all graphs except for Ref-100:0 display no variation in weight until 250 °C. Only above this temperature threshold degradation starts and progresses rapidly for all samples. The slight decline in weight experienced by Ref-100:0 could be attributed to evaporation of unreacted monomers within the network. Notably, the acrylate content of the networks influences the thermal degradation behavior – as indicated by the arrow in Figure 28. A higher amount of acrylate within the material leads to a higher weight loss during the first degradation step – which is biggest in Ref-100:0 and lowest in R-20:80. This is an indicator for the higher thermal stability of the epoxy-anhydride component.

R-50:50 and R-20:80 undergo three stages of degradation – the first one at a temperature of approximately 260 °C, a second one at about 50 % of remaining weight, and the last degradation stage happens after the switch to oxygen at 600 °C. Ref-100:0 and Ref-50:50 however only experience two degradation steps – the first one starting at 260 °C similarly to the other networks. The second degradation stage is only reached after the change of atmosphere above 600 °C. All samples show a nearly constant weight between 500 and 600 °C, before degradation is completed above 800 °C. The fact that there is an additional degradation step, which is accompanied by a temporary decrease in degradation speed in R-50:50 and R-20:80, indicates that the different monomers within the network formed have different thermal stability and degrade at different temperatures. Presumably, the acrylate network is mainly responsible for the first degradation step.

#### 4. Results and Discussion

All following experiments were performed below the temperature of beginning degradation of 250 °C.

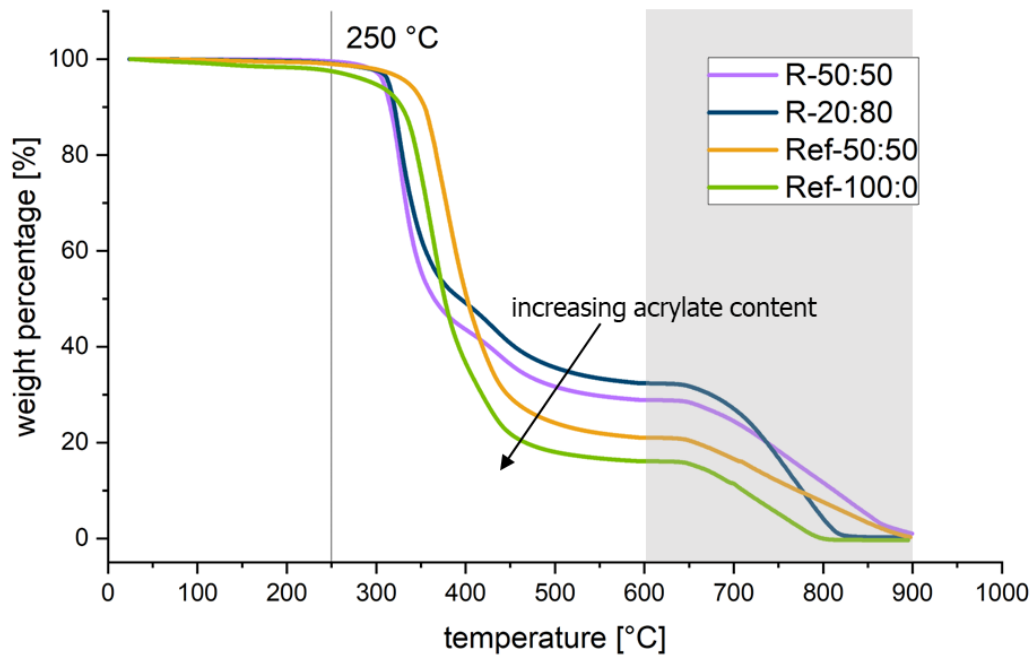


**Figure 28: percentage of weight loss over temperature for R-50:50, R-20:80, Ref-100:0 and Ref-50:50 (DGEBA instead of DGOA). The gray area indicates an oxygen atmosphere during measurement.**

## 4. Results and Discussion

### 4.2.2 DMA Measurements

DMA measurements were conducted to determine the  $T_g$  of the resins under investigation. By plotting  $\tan(\delta)$  against the sample temperature, the glass transition temperature of the samples can be obtained from the temperature at which the peak reaches its maximum.

Figure 29 plots the four formulations with varying acrylate content: R-50:50, R-40:60, R-30:70, and R-20:80. It is noticeable that the curve belonging to R-40:60 has an irregular behavior in the peak area, which can probably be attributed to instabilities during the measurement. As a consequence, the actual peak temperature – the  $T_g$  of the material – is likely to be higher in reality than the value listed in Table 5. The graph also shows that the peaks of  $\tan(\delta)$  lie in a similar temperature area for all four resins.

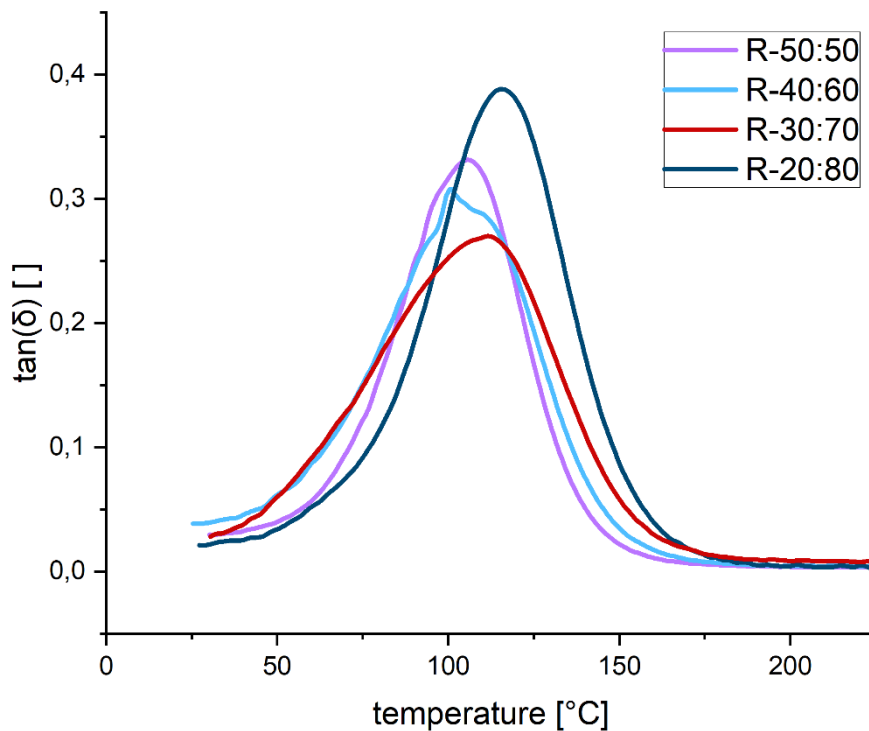


**Figure 29: comparison of  $\tan(\delta)$  over temperature for dual cured resins with varying acrylate content (R-50:50; R-40:60; R-20:80; R-30:70)**

In Figure 30 the resin R-50:50 is plotted together with the two reference formulations Ref-100:0 and Ref-50:50. As expected, the pure acrylate network (Ref-100:0) displays a peak at a considerably lower temperature than R-50:50. This is related to the fact that the acrylate network has a less rigid structure as well as a lower degree of crosslinking than the epoxy-anhydride network. As far as Ref-50:50 is concerned, the curve also shows signs of instabilities during the experiment. Nevertheless, it is evident that the  $T_g$  of Ref-50:50 is much higher than

#### 4. Results and Discussion

of the acrylate network and lies in the range of R-50:50. Even though the functionality of the reference epoxy is only two; the rigid chemical structure of DGEBA with two benzene rings causes a relatively high glass transition temperature.

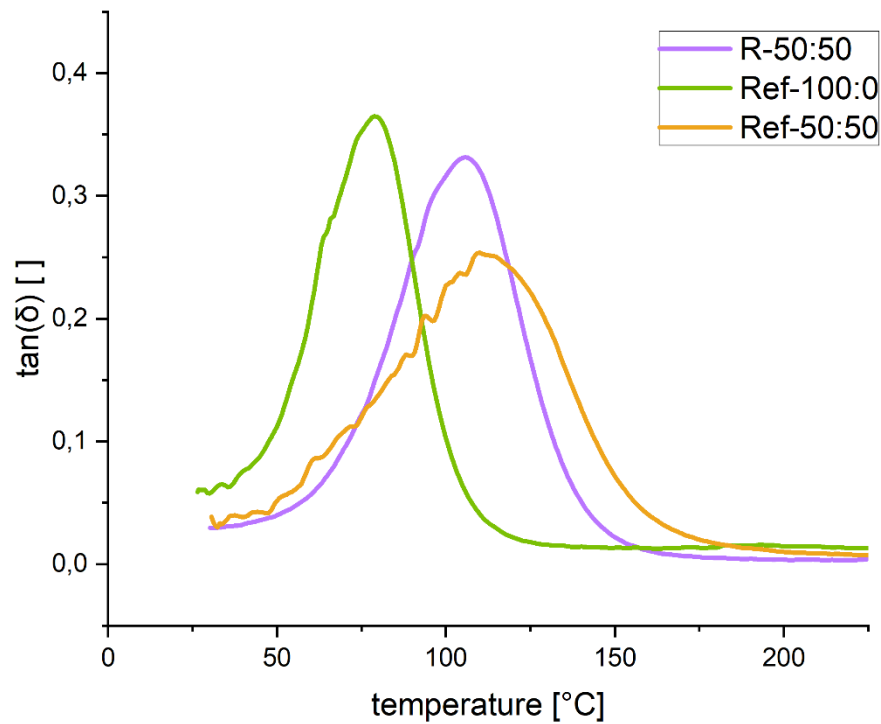


**Figure 30: comparison of  $\tan(\delta)$  over temperature for R-30:70 and the two reference formulations ratios Ref-100:0 and Ref-50:50 (DGEBA instead of DGOA))**

When contemplating the different curves, it is noteworthy that they show a singular peak of  $\tan(\delta)$  for each resin – even though all resins except for Ref-100:0 comprise two different chemical networks. Therefore, one might expect the networks to have two peaks. However, the behavior displayed indicates that the resins actually have a more homogenous structure that combines both networks, which leads to a singular  $T_g$  for the whole material [78]. Because the acrylate monomer bears three OH-groups, it is able to react with the epoxy monomer forming ether linkages [25]. Thus, chemical bonding between the two systems is possible and entails higher network homogeneity. In addition to the  $T_g$  also the width of the  $\tan(\delta)$  peak (full width at half maximum – FWHM) can be used to characterize the glass transition of a material. Homogenous materials exhibit a narrow glass transition whereas more heterogenous ones show a broader peak. The results of the DMA measurements are summarized in Table 5, which lists the full width at half maximum and the glass transition temperatures for each resin. It is apparent that Ref-100:0 exhibits the lowest FWHM – which can be expected as it only



#### 4. Results and Discussion

---

consists of an acrylate network and is therefore the most homogenous material. When increasing the amount of the epoxy-anhydride component in the resins, the resulting networks become less homogenous as the increasing width of the  $\tan(\delta)$  peak indicates [79]. R-20:80 noticeably shows a lower width than R-40:60 and R-30:70. The relatively high ratio of the epoxy-anhydride component possibly results in a more homogenous network, in which the acrylate component plays a less significant role. Especially R-40:60 and R-30:70 have high FWHM values, demonstrating that the combinations of the two chemical networks in these cases yield a more heterogenous network. Interestingly, Ref-50:50 exhibits the highest FWHM with 62 °C, which is significantly higher than the 42 °C of R-50:50. This could be caused by the absence of the tertiary amine which is catalyzing the epoxy-anhydride curing reaction. The curing mechanisms differ between the catalyzed and the uncatalyzed reaction. Literature suggests, that it is possible that the absence of a catalyst leads to a preference for epoxy homopolymerization [25]. Therefore, the heterogeneity of the network increases, as indicated by the high width of the  $\tan(\delta)$  peak.

The data shows that the  $T_g$  of the four DGOA-anhydride networks lies in a temperature range from 100 to 116 °C. Ref-100:0, however, has a glass transition temperature that is 20-35 °C lower than the  $T_g$  of the epoxy-containing resins. As observed previously, the peak of Ref-50:50 lies in close proximity to R-50:50.

**Table 5: full width at half maximum (FWHM) and glass transition temperatures**

resin name	FWHM [°C]	$T_g$ [°C]
R-50:50	42	106
R-40:60	56	100
R-30:70	60	112
R-20:80	48	116
Ref-100:0	36	79
Ref-50:50	62	110

In Figure 31, the glass transition temperatures of all resins except for Ref-50:50 are plotted against acrylate content. The straight lines have the purpose of acting as a guide for the eye only. As already mentioned above, the measurement of R-40:60 did not provide a reliable value. If R-40:60 – the value at 40 mol% acrylate content – is disregarded, a trend is visible

#### 4. Results and Discussion

---

in the diagram: With decreasing acrylate content – and therefore rising amount of epoxy-anhydride network in the material – the glass transition temperatures are rising. This behavior indicates that the epoxy-anhydride network that is formed during thermal curing affects the glass transition temperature positively.

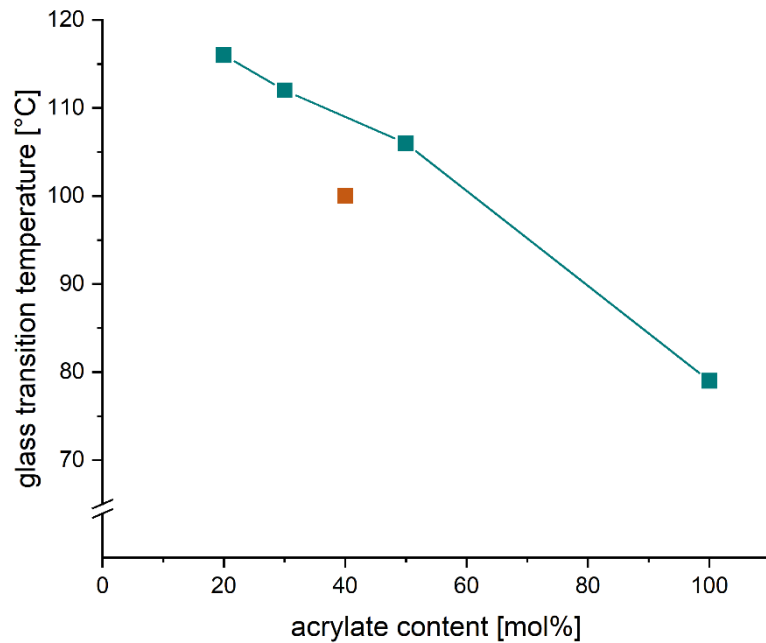


**Figure 31: glass transition temperatures plotted versus acrylate content**

### 4.3 Crosslinking Degree – Swelling Experiments

Swelling experiments were used to gain further insights into the formation of the thermally cured epoxy-anhydride network. Table 6 lists the gel contents for the samples that did not undergo thermal curing. The gel contents for the samples that underwent thermal curing are comprised in

Table 7. All values are averaged from three samples and are listed with the respective standard deviation.

**Table 6: gel content after each step - without thermal curing**

resin name	gel content [wt%]
R-50:50	50.84 ± 0.72
R-40:60	45.86 ± 1.41
R-30:70	40.42 ± 0.66
R-20:80	29.71 ± 1.76
Ref-100:0	87.87 ± 2.89
Ref-50:50	58.80 ± 2.85

**Table 7: gel content after each step - with thermal curing**

resin name	gel content [wt%]
R-50:50	101.91 ± 0.15
R-40:60	103.69 ± 0.43
R-30:70	101.20 ± 0.66
R-20:80	91.97 ± 0.44
Ref-100:0	100.66 ± 0.14
Ref-50:50	100.97 ± 0.08

#### 4. Results and Discussion

In order to illustrate the influence of the thermal curing step, the gel content was plotted against the acrylate content of the resins in Figure 32. The lines in the graph act as a guide for the eye. It is clearly evident from the blue marks that the gel content rises in accordance with the acrylate content of the respective samples. Therefore, it can be concluded that the acrylic network that is built during 3D-printing is insoluble and remains stable during the solvent exposure. The epoxy-anhydride network however is only formed in the thermal post-curing step; hence the monomers are still present in an unbound state and are susceptible to being dissolved. Swelling behavior after thermal curing is shown through the orange markers. The data shows that all resins except for R-20:80 have a remaining mass of over 100 % after drying – the excess can be attributed to incomplete drying of the swollen samples.

Due to the incomplete drying, no definite statement can be made concerning crosslink density. However, it is assumed that all samples have a gel content above 90 %. This hypothesis is also based on the results of the TGA measurements in chapter 4.2.1. No evaporation of volatile monomers could be detected except for R-100:0 until a temperature above 250 °C was reached. As R-20:80 shows poor printability, it is possible that the fragility of the samples after printing is not compensated by the epoxy-anhydride network in a way that leads to a completely insoluble network. This phenomenon could serve as an explanation for the fact that the original weight of the R-20:80 samples was not reached after drying. It can be presumed that the temperature of drying was too low at 60 °C – increased network mobility after surpassing the  $T_g$  might have led to complete drying.

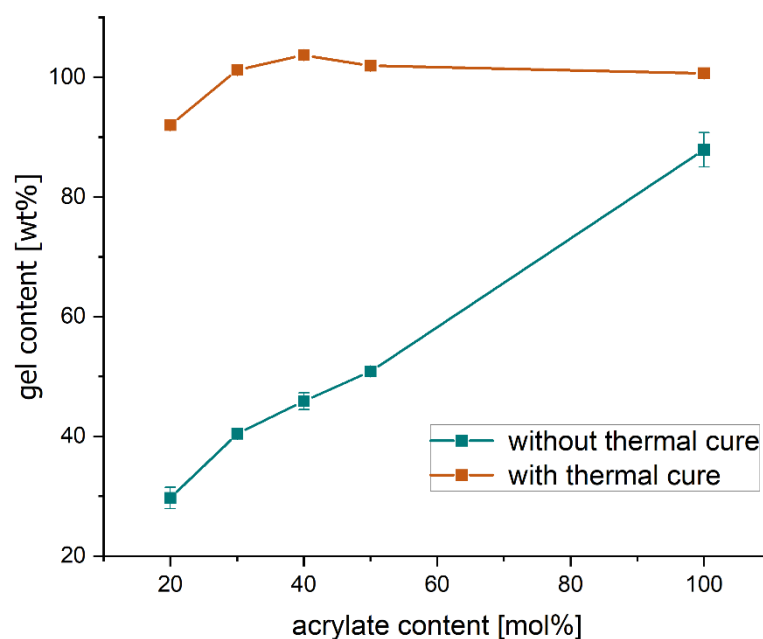


**Figure 32: gel content in dependence of the acrylate content**

### 4.4 Mechanical Properties

#### 4.4.1 Stress Relaxation

Stress relaxation experiments were performed to investigate the material flow of the different resins, which is enabled by catalyzed bond exchange reactions at elevated temperatures. The exchange reactions between free hydroxyl-groups and ester moieties enable relaxation of the networks, which can be analyzed by measuring the relaxation modulus  $G$  over time. Usually, the relaxation modulus is normalized to  $G/G_0$  – in which  $G_0$  is the initial value of  $G$ . The time at which  $G/G_0$  reaches  $1/e$  (=36.8 %) is termed characteristic relaxation time  $\tau^*$  according to the Maxwell model [80].

First, experiments were performed to compare the stress relaxation behavior under nitrogen atmosphere and under air for selected formulations. Figure 33 shows the two graphs for the resin R-20:80. It is apparent that the two curves are nearly identical, hence it can be assumed that the presence of air – and oxygen – does not influence the stress relaxation behavior. As a result, the decision was made to conduct the measurements under air – which also offered advantages in practicability and cost effectiveness.

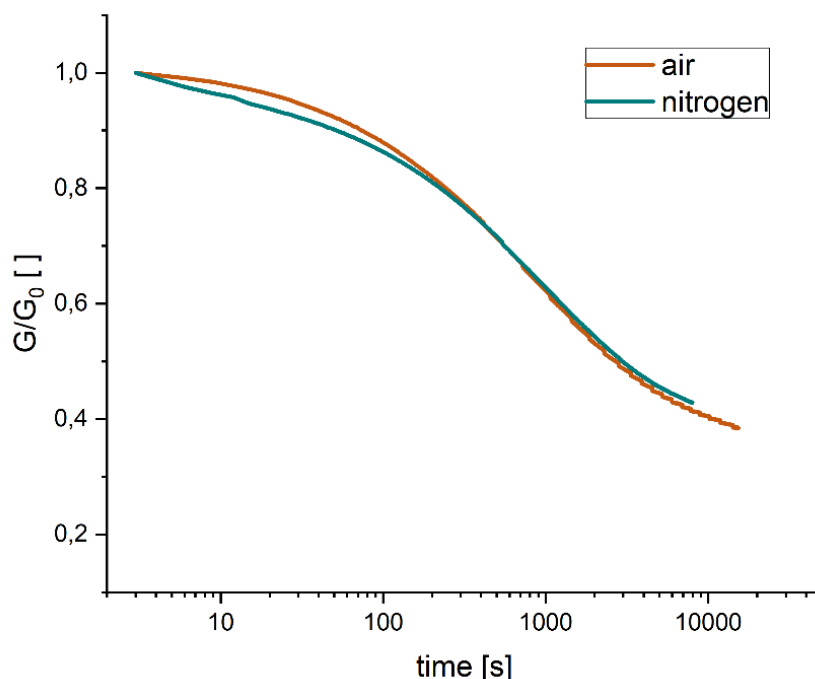


**Figure 33: comparison of rheological measurements under air and nitrogen atmosphere for R-20:80**

## 4. Results and Discussion

Figure 34 shows the stress relaxation behavior of the four networks with varying ratios of acrylate : epoxy-anhydride. Except for R-20:80 – which experiences a slower progressing stress relaxation than R-30:70 – it can be observed that the rate of change of the relaxation modulus increases with decreasing acrylate content. This behavior can be attributed to the fact that the epoxy monomer serves as a transesterification catalyst via its tertiary amine moiety. As the acrylate content goes down the epoxy-anhydride share of the resin rises – which in turn entails a higher catalyst concentration. From literature it is well known that the catalyst content influences the rate of exchange reactions. Generally, the more catalyst is used, the faster the stress relaxation occurs [57]. The slower relaxation of R-20:80 in comparison to R-30:70 could be caused by higher crosslinking, which could have a negative impact on stress relaxation behavior. The  $T_g$  of R-20:80 is at 116 °C whereas R-30:70 has a lower  $T_g$  of 112 °C – which can also be interpreted as an effect of a higher crosslinking degree in R-20:80. Gel content is another indicator for crosslinking degree – here R-20:80 exhibits a lower value (91.97 %) than R-30:70 (101.20 %). However, this could – as mentioned in chapter 4.3 – be attributed to the poor printability of R-20:80 leading to a rather porous structure. Beside the catalyst content, also the crosslinking degree has an influence on the rate of dynamic bond exchange reactions. It has been reported, that with increasing crosslinking degree the stress relaxation becomes slower if the same catalyst content and temperature are used [81].

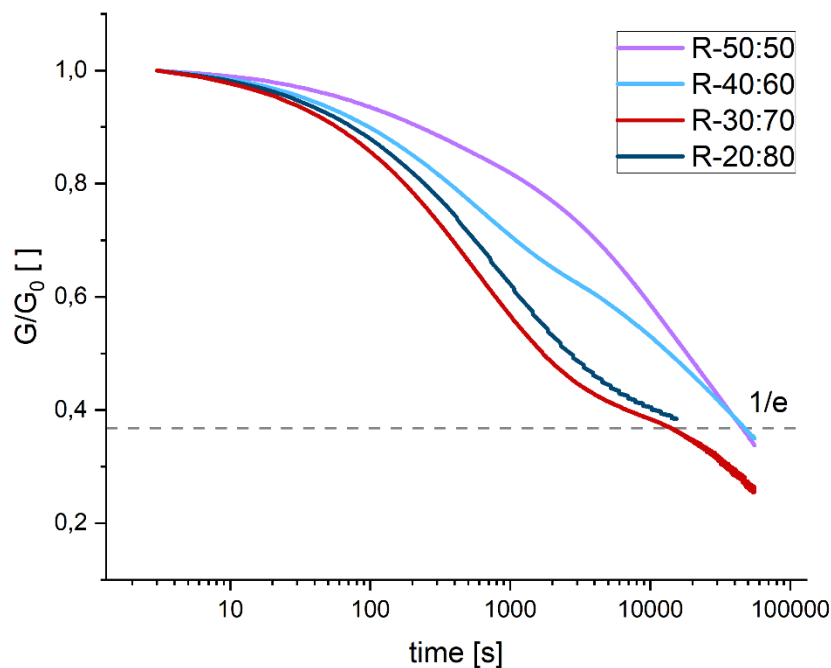


**Figure 34: stress relaxation behavior of R-50:50, R-40:60, R-30:70, and R-20:80**

#### 4. Results and Discussion

In Figure 35, a comparison of R-50:50 and the reference formulations Ref-100:0 and Ref-50:50 is shown. The curve of Ref-100:0 exhibits a dent in the end, which is due to instabilities during measurement, and the data does not reach  $1/e$  as measuring was stopped prematurely. Even though, it is clearly evident that stress relaxation in the sample with the acrylate network proceeds at a very slow rate. Residual stresses are often the result of acrylate curing, as they experience relatively high shrinkage due to their curing mechanism [48]. At temperatures above  $T_g$  polymeric materials undergo softening, which enables the reduction of residual stresses to some extent. This is the reason this reference sample experiences stress relaxation despite lacking a transesterification catalyst. Further, it is notable that R-50:50 exhibits a lower stress relaxation rate than Ref-50:50 in the beginning. Possibly, a reason for this phenomenon could be that the amount of catalyst in the R-50:50 network is too low to overcome the limitations of the highly crosslinked network completely. Another reason for the initially higher stress relaxation rate of Ref-50:50 could be higher internal stress caused by the curing reaction. However, the stress relaxation rate of the DGEBA-reference formulation appears to stay relatively constant in comparison to the other resins, therefore a very high characteristic relaxation time can be expected. The measurement for Ref-50:50 also was stopped too early to determine  $\tau^*$ .

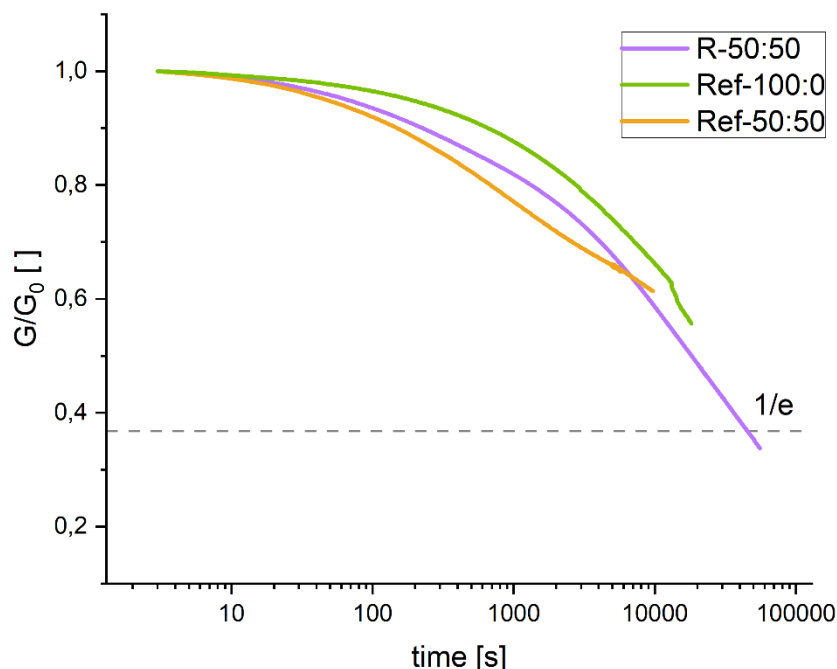


**Figure 35: stress relaxation behavior of R-50:50 and the two reference formulations Ref-100:0 and Ref-50:50 (DGEBA instead of DGOA)**

#### 4. Results and Discussion

From the stress relaxation measurements, the characteristic relaxation times of the resins were calculated and summarized in Table 8. For R-20:80,  $\tau^*$  was extrapolated, for Ref-100:0 and Ref-50:50 it was not possible to make an estimation as the measurements had to be ended before  $\tau^*$  was reached.

**Table 8: characteristic relaxation times of the different resins**

resin name	$\tau^*$ [s] / [min]
R-50:50	45420 / 757
R-40:60	47650 / 794
R-20:80	26000 / 433
R-30:70	14440 / 241
Ref-100:0	-
Ref-50:50	-

In addition to the data shown above, also the temperature dependence of stress relaxation was analyzed for the resin R-30:70. This material was chosen because it did exhibit the fastest stress relaxation in the previous experiment and good printability. Measurements were taken at four different temperatures – 200 °C, 210 °C, 220 °C, and 230 °C – the respective graphs are depicted in Figure 36 a). The characteristic relaxation times were derived from those measurements to generate an Arrhenius plot. For this purpose, the natural logarithm of all four  $\tau^*$  values was plotted over the reciprocal temperature, according to the Arrhenius law:

$$\tau(T) = \tau_0 * e^{\frac{E_a}{RT}}$$

In this equation,  $\tau$  is the relaxation time,  $T$  is the temperature,  $R$  is the universal gas constant and  $E_a$  equals the activation energy [2]. Figure 36 b) shows the resulting diagram. Additionally, a linear approximation was added to the graph, showing that the data fits a straight line with a Pearson correlation coefficient of 0.998. The straight-line fitting indicates that the data is in accordance with the Arrhenius law and therefore it can be claimed that the resin R-30:70 exhibits vitrimeric behavior.



## 4. Results and Discussion

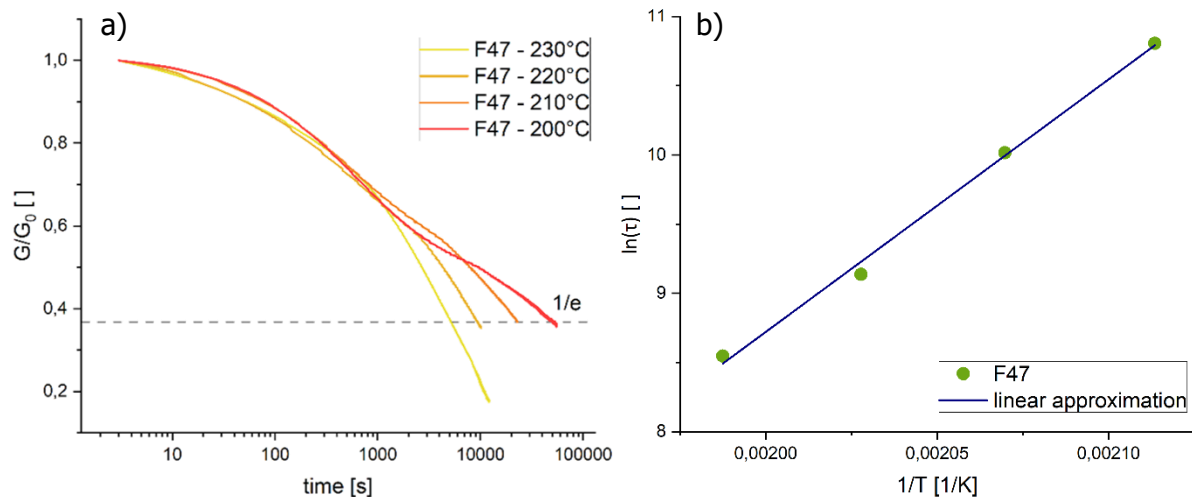


**Figure 36: temperature dependent stress relaxation of R-30:70 (a) and Arrhenius plot derived from those measurements (b)**

The Arrhenius plot was subsequently used to determine the topology freezing temperature  $T_v$  of the resin R-30:70. To achieve this, the averaged storage modulus of the rubbery plateau (determined through the DMA measurements) was used to calculate the characteristic relaxation time presuming a viscosity of  $10^{12}$  Pa s at  $T_v$ . The temperature at this  $\tau^*$  was calculated to be 211 °C using the Arrhenius plot – which equals  $T_v$  for R-30:70 – according to [82]. Applying the Arrhenius law, the activation energy  $E_a$  was determined via the slope  $m$  of the linear approximation ( $m = -E_a/R$ ), with  $R$  being the universal gas constant. Thus, an activation energy of 151.8 kJ/mol results. For epoxy-anhydride networks employing the very same epoxy monomer used in this thesis, activation energy values for a zinc(II)-acetylacetonate hydrate-catalyzed transesterification were found in literature [34]. The authors reported that their catalyzed networks show an activation energy between 53 and 87 kJ/mol. Their uncatalyzed reference network however exhibited an  $E_a$  of 154 kJ/mol – which is very similar to the value that was obtained in the present thesis. This shows that R-30:70 has a comparatively high activation energy, which can be explained through the high crosslink density of the network. Low mobility within the network is a result of the high crosslink density as well as the combination of the two networks. Therefore, higher energy input is needed for the transesterification reaction.

## 4. Results and Discussion

### 4.4.2 Tensile Testing

Tensile testing was performed on selected 3D-printed samples, namely R-30:70, Ref-100:0 and Ref-30:70. From each material, four samples were tested – the averaged results including the standard deviation for Young’s modulus  $E_t$ , tensile strength  $\sigma$ , and elongation at break  $\epsilon_b$  are listed in Table 9.

When comparing the values for the three parameters and the three materials, it is striking that Ref-30:70 displays not only a significantly lower modulus, but also tensile strength and strain at break provide much lower values. R-30:70 – containing 30 mol% of acrylates and 70 mol% of epoxy-anhydride mixture – however reaches the highest  $E_t$  of the tested materials, namely  $2550 \pm 91$  MPa. Additionally, its tensile strength also surpasses the other values with roughly 80 MPa. This shows that the epoxy monomers contribute largely to mechanical strength. However, the elongation at break is higher for the acrylate network of Ref-100:0. The chemical structure of the acrylate monomer – a long carbon chain bearing an acrylate group at each end – is much more flexible than the rigid epoxy monomer structure that involves a benzene ring. Naturally, this is also the case for the respective networks – the acrylate network exhibits higher flexibility and lower crosslink density. Also, its  $T_g$  which is significantly lower than the  $T_g$  of the networks containing an epoxy-anhydride component indicates a more flexible network. It is possible that the difference in crosslink density and chemical structure between DGEBA and DGOA is responsible for the disparity in mechanical behavior – DGEBA monomers exhibit a more rigid structure than the DGOA, e.g., caused by their benzene rings.

As mechanical properties are largely dependent on the mode of testing and also sample preparation and specimen type, it is difficult to compare the values at hand to those of other epoxy resins. To give an impression nevertheless, many commercial epoxy resins display a tensile strength of 80 MPa or lower – similar as the resin R-30:70. However, the Young’s modulus of those resins is usually above 3000 MPa.

**Table 9: results of tensile testing of the samples R-30:70, Ref-100:0, Ref-30:70 (DGEBA instead of DGOA)**

resin name	$E_t$	$\sigma$	$\epsilon_b$
R-30:70	$2550 \pm 91$	$79.7 \pm 1.7$	$4.52 \pm 0.18$
Ref-100:0	$2165 \pm 31$	$64.4 \pm 1.7$	$4.96 \pm 0.31$
Ref-30:70	$1498 \pm 85$	$22.6 \pm 1.2$	$1.89 \pm 0.21$

#### 4. Results and Discussion

Figure 37 depicts the stress-strain curves of all tensile tests. Two measurements of R-30:70 are in a lighter color as they appear to have experienced an error in data collection or clamping in the beginning. Both of them start with a negative strain. Apart from that they showcase the same behavior as the two remaining curves from the resin R-30:70. All other measurements display good reproducibility especially before reaching maximum stress. Deviations occurring can probably be attributed to minor faults of the specimens, e.g., small air pockets. The graph visualizes the notable differences in mechanical behavior of the resins.

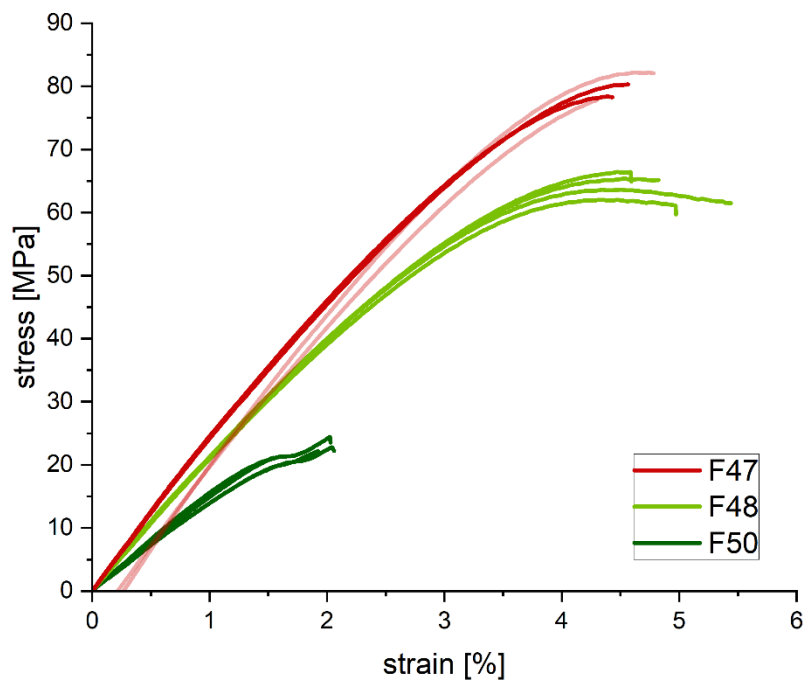


**Figure 37: stress-strain curves for all tested specimens from R-30:70, Ref-100:0, and Ref-30:70.**

Since samples were prepared via 3D-printing, the obtained results cannot be directly compared to values derived from measurements with standardized sample preparation. Often, 3D-printing leads to an anisotropic microstructure that is different from the structure obtained through other processes, e.g., injection molding, due to the layered build-up [83]. This is also reflected in anisotropic material properties. However, it can be assumed that based on the dual-cure approach a more homogenous structure is gained as the layer adhesion is improved. This is attributed to the thermal curing step, during which the formation of the epoxy-anhydride network takes place. Being exposed to temperature, the network development is not bound by any spatial constraints, thus contributing to a material structure that leans more toward isotropic behavior than materials solely processed through layered 3D-printing [44].

# 5 Summary and Outlook

Summarizing, different formulations consisting of a combination of acrylate and epoxy-anhydride networks were studied comparatively. The ratio of the two components was varied to gain insight into the influence of the resin composition on material properties. Aiming at creating a material with a  $T_g$  above 100 °C, decent printability, and vitrimeric behavior various experiments were performed.

First, curing behavior was analyzed through FTIR and DSC measurements to establish suitable curing conditions. After that DMA experiments were executed to analyze the  $T_g$ . It was found that the glass transition temperature increases with a rising share of the epoxy-anhydride network. Therefore, the focus was laid on achieving a highest possible  $T_g$  while still maintaining adequate processability. However, for the resin formulation containing only 20 mol% of acrylate monomers, the necessary printability was not given. When the acrylate share was heightened to 30 mol%, the quality of 3D-printing experienced an increase, while the  $T_g$  amounted to 112 °C. Further, the stress relaxation experiments showed that the tertiary amine group of the epoxy molecule is indeed able to catalyze the transesterification reaction, leading to dynamic networks. A higher amount of the epoxy-anhydride component in the resins seemed to accelerate stress relaxation due to better availability of the catalyst. Additionally, resin R-30:70 (acrylate : epoxy-anhydride = 30:70) performed best in the stress relaxation experiment, reaching a characteristic relaxation time of 241 min. Vitrimeric behavior was verified through an Arrhenius plot and a topology freezing temperature of 165 °C could be calculated. Through TGA measurements, thermal stability of the cured resin materials was proven until a temperature of 250 °C. In order to assess the mechanical properties of especially the resin with 30 mol% acrylate, tensile testing was performed. Displaying a Young's modulus of 2550 MPa, the resin also reached a higher tensile strength (80 MPa) than the reference materials.

As far as rapid tooling as a potential application is concerned, more material properties as well as parameters for processing have to be determined. Especially toughness is important to consider as an additional value to gain more insight into mechanical behavior. Therefore, it would be recommendable to do e.g., Charpy impact testing, as mechanical strength is required of tools to withstand high pressures during processing. Additionally, warpage needs to be looked into, as dimensional accuracy is necessary for applications in injection molding or extrusion. Hence, particularly the thermal curing step should be investigated from this angle.

## 5. Summary and Outlook

---

Moreover, the formation of interpenetrating networks is a topic for further discussion and investigation. Even though the DMA curves suggest a homogenous combination of both the acrylate and the epoxy-anhydride networks as there is only a singular peak in the  $\tan \delta$  curve, phase separation could still occur on nanoscale. Analysis with an atomic force microscope for instance could shine light on this possible phenomenon.

Concluding, the resin developed has potential to be a valuable candidate for rapid tooling. Due to the glass transition temperature determined, the processing of elastomers could offer a field of application – as processing temperatures are often not higher than 80 °C. Because pressures are especially high in injection molding, implementation for extrusion could be easier as the mechanical requirements are presumed to be lower.

# 6 Literature

- [1] A. Bagheri and J. Jin, "Photopolymerization in 3D Printing," *ACS Appl. Polym. Mater.*, vol. 1, no. 4, pp. 593–611, 2019, doi: 10.1021/acsapm.8b00165.
- [2] M. Capelot, M. M. Unterlass, F. Tournilhac, and L. Leibler, "Catalytic control of the vitrimer glass transition," *ACS Macro Lett.*, vol. 1, no. 7, pp. 789–792, 2012, doi: 10.1021/mz300239f.
- [3] A. Rosochowski and A. Matuszak, "Rapid tooling: the state of the art," *Mater. Process. Technol.*, vol. 106, pp. 191–198, 2000, doi: [https://doi.org/10.1016/S0924-0136\(00\)00613-0](https://doi.org/10.1016/S0924-0136(00)00613-0).
- [4] Y. Yagci, S. Jockusch, and N. J. Turro, "Photoinitiated polymerization: Advances, challenges, and opportunities," *Macromolecules*, vol. 43, no. 15, pp. 6245–6260, 2010, doi: 10.1021/ma1007545.
- [5] S. Chatani, C. J. Kloxin, and C. N. Bowman, "The power of light in polymer science: Photochemical processes to manipulate polymer formation, structure, and properties," *Polym. Chem.*, vol. 5, no. 7, pp. 2187–2201, 2014, doi: 10.1039/c3py01334k.
- [6] E. Schab-Balcerzak, E. Grabiec, D. Sęk, and A. Miniewicz, "New azobenzene chromophores as monomers for synthesis of polyesters," *Polym. J.*, vol. 35, no. 11, pp. 851–858, 2003, doi: 10.1295/polymj.35.851.
- [7] B. Wardle, *Principles and Applications of Photochemistry*. Manchester, UK: John Wiley, 2009.
- [8] W. Schnabel, *Polymers and Light: Fundamentals and Technical Applications*. Weinheim: WILEY-VCH Verlag GmbH & Co. KGaA, 2007.
- [9] A. Albin, "Norrish ' type I and II reactions and their role in the building of photochemical science," *Photochem. Photobiol. Sci.*, vol. 20, no. 1, pp. 161–181, 2021, doi: 10.1007/s43630-020-00003-9.
- [10] A. Stiles, T. Tison, L. Pruitt, and U. Vaidya, "Photoinitiator Selection and Concentration in Photopolymer Formulations towards Large-Format Additive Manufacturing," pp. 1–24, 2022.
- [11] Z. Szablan, T. M. Lovestead, T. P. Davis, M. H. Stenzel, and C. Barner-kowollik, "Mapping Free Radical Reactivity : A High-Resolution Electrospray Ionization - Mass Spectrometry Study of Photoinitiation Processes in Methyl Methacrylate Free Radical Polymerization," pp. 26–39, 2007.
- [12] S. Benedikt *et al.*, "Highly Efficient Water-Soluble Visible Light Photoinitiators," pp. 473–479, 2016, doi: 10.1002/pola.27903.
- [13] C. Barner-Kowollik, "Acrylate free radical polymerization: From mechanism to polymer design," *Macromol. Rapid Commun.*, vol. 30, no. 23, pp. 1961–1963, 2009, doi: 10.1002/marc.200900676.
- [14] G. Odian, *Principles of Polymerization*, 4th editio. New York: John Wiley & Sons, Inc., 2004.
- [15] J. Wu *et al.*, "Evolution of material properties during free radical photopolymerization," *J. Mech. Phys. Solids*, vol. 112, pp. 25–49, 2018, doi:

## 6. Literature

---

- 10.1016/j.jmps.2017.11.018.
- [16] K. J. Saunders, *Organic Polymer Chemistry*, 2nd editio. London, New York: Chapman and Hall, 1988.
- [17] A. M. Van Herk, "Historic Account of the Development in the Understanding of the Propagation Kinetics of Acrylate Radical Polymerizations," pp. 1964–1968, 2009, doi: 10.1002/marc.200900574.
- [18] N. Ballard and J. M. Asua, "Radical polymerization of acrylic monomers: An overview," *Prog. Polym. Sci.*, vol. 79, pp. 40–60, 2018, doi: 10.1016/j.progpolymsci.2017.11.002.
- [19] S. C. Ligon, B. Husár, H. Wutzel, R. Holman, and R. Liska, "Strategies to reduce oxygen inhibition in photoinduced polymerization," *Chem. Rev.*, vol. 114, no. 1, pp. 577–589, 2014, doi: 10.1021/cr3005197.
- [20] C. E. Hoyle, T. Y. Lee, and T. Roper, "Thiol-enes: Chemistry of the past with promise for the future," *J. Polym. Sci. Part A Polym. Chem.*, vol. 42, no. 21, pp. 5301–5338, 2004, doi: 10.1002/pola.20366.
- [21] P. Dubois, O. Coulembier, and J.-M. Raquez, *Handbook of Ring-Opening Polymerization*. Weinheim: WILEY-VCH Verlag GmbH & Co. KGaA, 2009.
- [22] T. Vidil, F. Tournilhac, S. Musso, A. Robisson, and L. Leibler, "Control of reactions and network structures of epoxy thermosets," pp. 1–54, 2016, doi: 10.1016/j.progpolymsci.2016.06.003.
- [23] B. Ellis, *Chemistry and Technology of Epoxy Resins*, First edit. Springer Science+Business Media Dordrecht, 1993.
- [24] J. Rocks, "Characterization of Novel Co-Anhydride cured Epoxy Resins," *Technology*, p. 190, 2004.
- [25] A. I. Barabanova, B. V. Lokshin, E. P. Kharitonova, E. S. Afanasyev, A. A. Askadskii, and O. E. Philippova, "Curing cycloaliphatic epoxy resin with 4-methylhexahydrophthalic anhydride: Catalyzed vs . uncatalyzed reaction," *Polymer (Guildf.)*, vol. 178, no. April, p. 121590, 2019, doi: 10.1016/j.polymer.2019.121590.
- [26] A. N. Mauri and C. C. Riccardi, "The Effect of Epoxy Excess on the Kinetics of an Epoxy – Anhydride System," pp. 2342–2349, 2002, doi: 10.1002/app.10867.
- [27] B. Bilyeu, W. Brostow, and K. P. Menard, "Epoxy Thermosets and their Applications. II. Thermal Analysis," vol. 22, pp. 107–129, 2000.
- [28] O. Nuyken and S. D. Pask, "Ring-Opening Polymerization—An Introductory Review," pp. 361–403, 2013, doi: 10.3390/polym5020361.
- [29] L. Matejka, J. Lovy, S. Pokorny, K. Bouchal, and K. Dusek, "Curing Epoxy Resins With Anhydrides. Model Reactions and Reaction Mechanism.," *J. Polym. Sci. A1.*, vol. 21, no. 10, pp. 2873–2885, 1983, doi: 10.1002/pol.1983.170211003.
- [30] G. Couture *et al.*, "Limonene-Based Epoxy: Anhydride Thermoset Reaction Study," no. Scheme 1, pp. 1–16, 2018, doi: 10.3390/molecules23112739.
- [31] J. Rocks, L. Rintoul, F. Vohwinkel, and G. George, "The kinetics and mechanism of cure of an amino-glycidyl epoxy resin by a co-anhydride as studied by FT-Raman spectroscopy," vol. 45, pp. 6799–6811, 2004, doi:

## 6. Literature

---

- 10.1016/j.polymer.2004.07.066.
- [32] J. Leukel, W. Burchard, R.-P. Krüger, H. Much, and G. Schulz, "Mechanism of the anionic copolymerization of anhydride-cured epoxies - analyzed by matrix-assisted laser desorption ionization time-of-flight mass spectrometry," vol. 366, pp. 359–366, 1996.
- [33] P. Musto, M. Abbate, G. Ragosta, and G. Scarinzi, "A study by Raman, near-infrared and dynamic-mechanical spectroscopies on the curing behaviour, molecular structure and viscoelastic properties of epoxy / anhydride networks," vol. 48, 2007, doi: 10.1016/j.polymer.2007.04.042.
- [34] M. Giebler, C. Sperling, S. Kaiser, I. Duretek, and S. Schlögl, "Epoxy-anhydride vitrimers from aminoglycidyl resins with high glass transition temperature and efficient stress relaxation," *Polymers (Basel)*, vol. 12, no. 5, pp. 1–14, 2020, doi: 10.3390/POLYM12051148.
- [35] J. R. Millar, "Interpenetrating Polymer Networks. Styrene-Divinylbenzene Copolymers with Two and Three Interpenetrating Networks, and Their Sulphonates," pp. 1311–1317, 1960, doi: <https://doi.org/10.1039/JR9600001311>.
- [36] U. Farooq, J. Teuwen, and C. Dransfeld, "Toughening of Epoxy Systems with Interpenetrating Polymer Network (IPN): A Review," *Polymers (Basel)*, vol. 12, no. 1908, 2020, doi: 10.3390/polym12091908.
- [37] L. H. Sperling, A. A. Baidak, and J. M. Liégeois, "Simultaneous Interpenetrating Polymer Networks Based on Epoxy – Acrylate Combinations," pp. 1973–1984, 2014.
- [38] M. S. Silverstein, "Interpenetrating polymer networks: So happy together?," *Polymer (Guildf)*, vol. 207, no. April, p. 122929, 2020, doi: 10.1016/j.polymer.2020.122929.
- [39] Y. S. Lipatov and T. Alekseeva, "Phase-Separated Interpenetrating Polymer Networks," *Adv. Polym. Sci.*, no. September, pp. 1–227, 2007, doi: DOI 10.1007/12\_2007\_116.
- [40] S. Lantean, I. Roppolo, M. Sangermano, C. F. Pirri, and A. Chiappone, "Development of new hybrid acrylic/epoxy DLP-3D printable materials," *Inventions*, vol. 3, no. 2, pp. 1–13, 2018, doi: 10.3390/inventions3020029.
- [41] L. H. Sperling and R. Hu, *Polymer Blends Handbook*, 2nd ed. Springer Science+Business Media Dordrecht, 2014.
- [42] J. R. Nowers, J. A. Costanzo, and B. Narasimhan, "Structure – Property Relationships in Acrylate / Epoxy Interpenetrating Polymer Networks: Effects of the Reaction Sequence and Composition," *Appl. Polym. Sci.*, vol. 104, pp. 891–901, 2007, doi: 10.1002/app.
- [43] O. Konuray, X. Fernández-Francos, X. Ramis, and À. Serra, "State of the Art in Dual-Curing Acrylate Systems," *Polymers (Basel)*, vol. 10, no. 178, 2018, doi: 10.3390/polym10020178.
- [44] X. Fernández-Francos, O. Konuray, X. Ramis, À. Serra, and S. De la Flor, "Enhancement of 3D-Printable Materials by Dual-Curing Procedures," *Materials (Basel)*, vol. 14, no. 107, 2021, doi: <https://doi.org/10.3390/ma14010107>.



## 6. Literature

---

- [45] C. Park, S. Lee, J. Park, and H. Kim, "Preparation and characterization of dual curable adhesives containing epoxy and acrylate functionalities," *React. Funct. Polym.*, vol. 73, no. 4, pp. 641–646, 2013, doi: 10.1016/j.reactfunctpolym.2013.01.012.
- [46] X. Kuang, Z. Zhao, K. Chen, D. Fang, and G. Kang, "High-Speed 3D Printing of High-Performance Thermosetting Polymers via Two-Stage Curing," *Macromol. Rapid Commun.*, vol. 1700809, pp. 1–8, 2018, doi: 10.1002/marc.201700809.
- [47] I. Cazin, M. O. Gleirscher, M. Fleisch, M. Berer, M. Sangermano, and S. Schlögl, "Spatially controlling the mechanical properties of 3D printed objects by dual-wavelength vat photopolymerization," *Addit. Manuf.*, vol. 57, no. May, 2022, doi: 10.1016/j.addma.2022.102977.
- [48] O. Konuray, J. M. Salla, J. M. Morancho, X. Fernández-Francos, M. García-Alvarez, and X. Ramis, "Curing kinetics of acrylate-based and 3D printable IPNs," *Thermochim. Acta*, vol. 692, no. August, p. 178754, 2020, doi: 10.1016/j.tca.2020.178754.
- [49] D. Montarnal, M. Capelot, F. Tournilhac, and L. Leibler, "Silica-like malleable materials from permanent organic networks," *Science (80-. )*, vol. 334, no. 6058, pp. 965–968, 2011, doi: 10.1126/science.1212648.
- [50] C. N. Bowman and C. J. Kloxin, "Covalent adaptable networks: Reversible bond structures incorporated in polymer networks," *Angew. Chemie - Int. Ed.*, vol. 51, no. 18, pp. 4272–4274, 2012, doi: 10.1002/anie.201200708.
- [51] Q. Chen, X. Yu, Z. Pei, Y. Yang, Y. Wei, and Y. Ji, "Multi-stimuli responsive and multi-functional oligoaniline-modified vitrimers," *Chem. Sci.*, pp. 724–733, 2017, doi: 10.1039/c6sc02855a.
- [52] W. Denissen, J. M. Winne, and F. E. Du Prez, "Vitrimers: Permanent organic networks with glass-like fluidity," *Chem. Sci.*, vol. 7, no. 1, pp. 30–38, 2016, doi: 10.1039/c5sc02223a.
- [53] J. M. Winne, L. Leibler, and F. E. Du Prez, "Dynamic covalent chemistry in polymer networks: A mechanistic perspective," *Polym. Chem.*, vol. 10, no. 45, pp. 6091–6108, 2019, doi: 10.1039/c9py01260e.
- [54] W. Denissen, G. Rivero, R. Nicolaÿ, L. Leibler, J. M. Winne, and F. E. Du Prez, "Vinyllogous urethane vitrimers," *Adv. Funct. Mater.*, vol. 25, no. 16, pp. 2451–2457, 2015, doi: 10.1002/adfm.201404553.
- [55] M. M. Obadia *et al.*, "Reprocessing and Recycling of Highly Cross-Linked Ion-Conducting Networks through Transalkylation Exchanges of C – N Bonds," 2015, doi: 10.1021/jacs.5b02653.
- [56] G. B. Lyon, L. M. Cox, J. T. Goodrich, A. D. Baranek, Y. Ding, and C. N. Bowman, "Remoldable Thiol-Ene Vitrimers for Photopatterning and Nanoimprint Lithography," *Macromolecules*, vol. 49, no. 23, pp. 8905–8913, 2016, doi: 10.1021/acs.macromol.6b01281.
- [57] E. Rossegger *et al.*, "High resolution additive manufacturing with acrylate based vitrimers using organic phosphates as transesterification catalyst," *Polymer (Guildf)*, 2021, doi: 10.1016/j.polymer.2021.123631.
- [58] B. Zhang, K. Kowsari, A. Serjouei, M. L. Dunn, and Q. Ge, "Reprocessable

## 6. Literature

---

- thermosets for sustainable three-dimensional printing,” *Nat. Commun.*, vol. 9, no. 1, 2018, doi: 10.1038/s41467-018-04292-8.
- [59] F. I. Altuna, C. E. Hoppe, and R. J. J. Williams, “Epoxy vitrimers: The effect of transesterification reactions on the network structure,” *Polymers (Basel)*, vol. 10, no. 1, 2018, doi: 10.3390/polym10010043.
- [60] A. Demongeot, S. J. Mougner, S. Okada, C. Soulié-Ziakovic, and F. Tournilhac, “Coordination and catalysis of Zn<sup>2+</sup> in epoxy-based vitrimers,” *Polym. Chem.*, vol. 7, no. 27, pp. 4486–4493, 2016, doi: 10.1039/c6py00752j.
- [61] J. Han, T. Liu, C. Hao, S. Zhang, B. Guo, and J. Zhang, “A Catalyst-Free Epoxy Vitriimer System Based on Multifunctional Hyperbranched Polymer,” *Macromolecules*, vol. 51, no. 17, pp. 6789–6799, 2018, doi: 10.1021/acs.macromol.8b01424.
- [62] F. I. Altuna, C. E. Hoppe, and R. J. J. Williams, “Epoxy vitrimers with a covalently bonded tertiary amine as catalyst of the transesterification reaction,” *Eur. Polym. J.*, vol. 113, no. January, pp. 297–304, 2019, doi: 10.1016/j.eurpolymj.2019.01.045.
- [63] T. Liu *et al.*, “A Self-Healable High Glass Transition Temperature Bioepoxy Material Based on Vitriimer Chemistry,” *Macromolecules*, vol. 51, no. 15, pp. 5577–5585, 2018, doi: 10.1021/acs.macromol.8b01010.
- [64] Z. Ma, Y. Wang, J. Zhu, J. Yu, and Z. Hu, “Bio-based epoxy vitrimers: Reprocessibility, controllable shape memory, and degradability,” *J. Polym. Sci. Part A Polym. Chem.*, vol. 55, no. 10, pp. 1790–1799, 2017, doi: 10.1002/pola.28544.
- [65] Q. Shi *et al.*, “Recyclable 3D printing of vitriimer epoxy,” *Mater. Horizons*, vol. 4, no. 4, pp. 598–607, 2017, doi: 10.1039/c7mh00043j.
- [66] I. Gibson, D. Rosen, and B. Stucker, *Additive Manufacturing Technologies*, 2nd Editio. New York: Springer Science+Business Media New York, 2015.
- [67] E. Rossegger *et al.*, “Digital light processing 3D printing with thiol–acrylate vitrimers,” *Polym. Chem.*, vol. 12, pp. 639–644, 2021, doi: 10.4324/9781315079097-35.
- [68] H. Kadry, S. Wadnap, C. Xu, and F. Ahsan, “Digital light processing (DLP) 3D-printing technology and photoreactive polymers in fabrication of modified-release tablets,” *Eur. J. Pharm. Sci.*, vol. 135, no. April, pp. 60–67, 2019, doi: 10.1016/j.ejps.2019.05.008.
- [69] M. Layani, X. Wang, and S. Magdassi, “Novel Materials for 3D Printing by Photopolymerization,” *Adv. Mater.*, vol. 30, no. 41, pp. 1–7, 2018, doi: 10.1002/adma.201706344.
- [70] G. Katal, N. Tyagi, and A. Joshi, “Digital Light Processing and its Future Applications,” *Int. J. Sci. Res. Publ.*, vol. 3, no. 4, pp. 330–337, 2013.
- [71] D. T. Pham and S. S. Dimov, *Rapid Manufacturing*. Cardiff: Springer-Verlag London Limited, 2011.
- [72] K. Ch. Chua, K. F. Leong, and Z. H. Liu, *Handbook of Manufacturing Engineering and Technology*, 1st Editio. Springer-Verlag London, 2015.

## 6. Literature

---

- [73] R. Mau *et al.*, “Rapid tooling for micro injection molding of micro medical devices via digital light processing,” vol. 3, no. 1, pp. 2–3, 2021, doi: 10.18416/AMMM.2021.2109537.
- [74] A. Equbal, A. Kumar, and M. Shamim, “Rapid tooling: A major shift in tooling practice Rapid Tooling,” *J. Manuf. Ind. Eng.*, no. December, 2015, doi: 10.12776/mie.v14i3-4.325.
- [75] S. L. Agius, M. Joosten, B. Trippit, C. H. Wang, and T. Hilditch, “Part A Rapidly cured epoxy / anhydride composites: Effect of residual stress on laminate shear strength,” *Compos. Part A*, vol. 90, pp. 125–136, 2016, doi: 10.1016/j.compositesa.2016.06.013.
- [76] C. N. Bowman and C. J. Kloxin, “Toward an Enhanced Understanding and Implementation of Photopolymerization Reactions,” *AIChE J.*, vol. 54, no. 4, pp. 2775–2795, 2008, doi: 10.1002/aic.
- [77] O. Konuray, J. M. Morancho, X. Fernández-Francos, M. García-Alvarez, and X. Ramis, “Curing kinetics of dually-processed acrylate-epoxy 3D printing resins,” *Thermochim. Acta*, vol. 701, no. May, 2021, doi: 10.1016/j.tca.2021.178963.
- [78] A. Roig, X. Ramis, S. De la Flor, and À. Serra, “Sequential photo-thermal curing of (meth)acrylate-epoxy thiol formulations,” *Polymer (Guildf)*., vol. 230, 2021, doi: 10.1016/j.polymer.2021.124073.
- [79] X. Zhang, L. Cox, Z. Wen, W. Xi, Y. Ding, and C. N. Bowman, “Implementation of two distinct wavelengths to induce multistage polymerization in shape memory materials and nanoimprint lithography,” *Polymer (Guildf)*., vol. 156, no. July, pp. 162–168, 2018, doi: 10.1016/j.polymer.2018.09.032.
- [80] W. Denissen, M. Driesbeke, R. Nicola, L. Leibler, J. M. Winne, and F. E. Du Prez, “Chemical control of the viscoelastic properties of vinylogous urethane vitrimers,” *Nat. Commun.*, vol. 8, 2017, doi: 10.1038/ncomms14857.
- [81] Y. Liu *et al.*, “Tuning the mechanical and dynamic properties of imine bond crosslinked elastomeric vitrimers by manipulating the crosslinking degree,” *Polym. Chem.*, 2020, doi: 10.1039/C9PY01826C.
- [82] W. Alabiso, T. M. Hron, D. Reisinger, D. Bautista-anguís, and S. Schlögl, “Shape memory-assisted self-healing of dynamic thiol-acrylate networks,” pp. 5704–5714, 2021, doi: 10.1039/d1py00925g.
- [83] M. Monzón, Z. Ortega, A. Hernández, R. Paz, and F. Ortega, “Anisotropy of Photopolymer Parts Made by Digital Light Processing,” *Materials (Basel)*., no. Figure 1, pp. 1–15, 2017, doi: 10.3390/ma10010064.

## 7 Abbreviations and Symbols

Abbreviation	Meaning	Unit
A	absorbance of irradiation	
$A_0$	absorption area – peak of uncured sample	
AMT	additive manufacturing technology	
$A_{\text{peak}}$	absorption area – peak of cured sample	
$A_{\text{Ref}}$	absorption area – reference peak, cured	
$A_{\text{Ref.0}}$	absorption area – reference peak, uncured	
BAPO	bis(2,4,6-trimethylbenzoyl)-phenylphosphine oxide	
C	conversion	
CAD	computer aided design	
CAN	covalent adaptable materials	
d	length of optical path	m
DCM	dichloromethane	
DGEBA	bisphenol-A-diglycidyl-ether	
DGOA	<i>N,N</i> -diglycidyl-4-glycidylloxylaniline	
DLP	digital light processing	
DMA	dynamic mechanical analysis	
DSC	differential scanning calorimetry	
E	energy	J
e.g.	exempli gratia	
$E_a$	activation energy	J/mol
$E_t$	Young's modulus (tensile)	MPa
et al.	et alia; and others	
FTIR	Fourier-transform infrared spectroscopy	
FWHM	full width at half maximum	°C
G	relaxation modulus	MPa
$G_0$	initial relaxation modulus	MPa
GDGDA	glycerol 1,3-diglycerolate diacrylate	
h	Planck's constant	$\text{m}^2\text{kg}\cdot\text{s}^{-1}$
HOMO	highest occupied molecular orbital	

## 7. Abbreviations and Symbols

---

I	emergent intensity	W/m <sup>2</sup>
i.e.	id est	
I <sub>0</sub>	incident intensity	W/m <sup>2</sup>
I <sub>A</sub>	absorbed intensity	W/m <sup>2</sup>
ic	internal conversion	
ICN	interconnected network	
IPN	interpenetrating network	
isc	intersystem crossing	
LED	light emitting diode	
LUMO	lowest unoccupied molecular orbital	
m	slope	
MNA	methyl-5-norbornene-2,3-dicarboxylic anhydride	
mol%	molar percentage	%
R	universal gas constant	JK <sup>-1</sup> mol <sup>-1</sup>
R <sub>i</sub>	initiation rate	
ROP	ring opening polymerization	
RP	rapid prototyping	
RT	rapid tooling	
S <sub>0</sub>	ground state	
S <sub>1</sub>	excited state	
S <sub>2</sub>	excited state	
SLA	stereolithography	
T	temperature	°C
T <sub>1</sub>	triplet state	
tan(δ)	dissipation factor	
TBD	1,5,7-triazabicyclo[4.4.0]dec-5-ene	
T <sub>g</sub>	glass transition temperature	°C
TGA	thermogravimetric analysis	
TPO-L	ethyl (2,4,6-trimethylbenzoyl)-phenyl phosphinate	
T <sub>v</sub>	topology freezing temperature	°C
US	United States of America	
UV	ultraviolet	

## 7. Abbreviations and Symbols

---

v	vibrational state	
$\nu_r$	vibrational relaxation	
w	weight after drying	mg
$w_0$	original weight	mg
WLF	Williams-Landel-Ferry	
wt%	weight percentage	%
$\Delta H$	enthalpy of reaction	J/mol
$\epsilon$	molecular extinction coefficient	$\text{Lmol}^{-1}\text{cm}^{-1}$
$\epsilon_b$	elongation at break	%
$\nu$	oscillation frequency	$\text{s}^{-1}$
$\sigma$	tensile strength	MPa
$\tau$	relaxation time	s
$\tau^*$	characteristic relaxation time	s
$\phi$	quantum yield	

## 8 List of Tables

Table 1: used chemicals .....	31
Table 2: instruments used .....	32
Table 3: resin formulations under investigation.....	33
Table 4: printing settings.....	34
Table 5: full width at half maximum (FWHM) and glass transition temperatures.....	51
Table 7: gel content after each step - without thermal curing.....	53
Table 8: gel content after each step - with thermal curing .....	53
Table 6: characteristic relaxation times of the different resins .....	58
Table 9: results of tensile testing of the samples R-30:70, Ref-100:0, Ref-30:70 (DGEBA instead of DGOA) .....	60

## 9 Table of Figures

Figure 1: HOMO - LUMO - transition (adapted from [8]) .....	4
Figure 2: schematic Jablonski diagram (adapted from [7]). Abbreviations: ic - internal conversion; isc - intersystem crossing; vr - vibration-relaxation.....	5
Figure 3: molecular structures of benzoin, BAPO, and TPO-L (from left to right).....	7
Figure 4: scheme of a chain growth polymerization .....	8
Figure 5: chemical structures of a generic acrylate (left) and of glycerol 1,3-diglycerolate diacrylate (right) .....	9
Figure 6: general structure of an epoxy group (left) and N, N-diglycidyl-4-glycidyoxyaniline (DGOA, middle) and bisphenol-A-diglycidyl-ether (right), both epoxies used in this thesis .	12
Figure 7: epoxy homopolymerization – etherification reaction between alkoxide ion and epoxy molecule .....	13
Figure 8: general mechanism of anionic ROP, adapted from [21].....	14
Figure 9: general structure of a carboxylic acid anhydride (left) and structure of methyl-5-norbornene-2,3-dicarboxylic anhydride (MNA) (right) .....	15
Figure 10: formation of a zwitterion from the reaction of epoxide with tertiary amine .....	16
Figure 11: formation of a carboxylate ion through the reaction of alkoxide .....	16
Figure 12: carboxylate anion reacts with epoxy, leading to chain propagation .....	16
Figure 13: schematic illustration of the difference between sequential IPNs (seq-IPN) and simultaneous IPN (sim-IPN), adapted from [38]. Abbreviations: M <sub>1</sub> - monomer 1; C <sub>1</sub> - crosslinker 1; R <sub>1</sub> - reaction 1; M <sub>2</sub> - monomer 2; C <sub>2</sub> - crosslinker 2; R <sub>2</sub> - reaction 2.....	18
Figure 14: comparison of the structures: IPN, ICN, semi-IPN, adapted from [38] .....	19
Figure 15: exemplary dual curing process, adapted from [43] .....	21
Figure 16: schematic crosslink interchange of an associative network, adapted from [53] .....	22
Figure 17: schematic crosslink interchange in a dissociative CAN, adapted from [53].....	23
Figure 18: left: Arrhenius dependent behavior of viscosity in proximity of T <sub>v</sub> as with vitrimers; right: viscosity graph of a thermoplastic polymer above T <sub>g</sub> ; figure adapted from [2].....	24
Figure 19: schematic illustration of a transesterification reaction.....	25
Figure 20: simplified illustration of the DLP process, adapted from [57].....	28



## 9. Table of Figures

---

Figure 21: DSC curves of the first and second heat run of R-50:50 .....	39
Figure 22: DSC curves of the first and second heat run of R-30:70 .....	40
Figure 23: isothermal curing of R-30:70 (30:70) at 150 °C.....	41
Figure 24: Conversion of the acrylate band at 1635 cm <sup>-1</sup> plotted against curing time. ....	43
Figure 25: Conversion of the epoxy band at 912 cm <sup>-1</sup> plotted against curing time. After 20 min, the curing temperature switches from 80 °C to 150 °C. ....	44
Figure 26: FTIR spectra recorded before and after illumination for 300 s at 405 nm for the resin formulation R-30:70 .....	45
Figure 27: FTIR spectra recorded after illumination for 300 s at 405 nm and after each thermal curing step for the resin formulation R-30:70.....	45
Figure 28: percentage of weight loss over temperature for R-50:50, R-20:80, Ref-100:0 and Ref- 50:50 (DGEBA instead of DGOA). The gray area indicates an oxygen atmosphere during measurement. ....	48
Figure 29: comparison of tan(δ) over temperature for dual cured resins with varying acrylate content (R-50:50; R-40:60; R-20:80; R-30:70) .....	49
Figure 30: comparison of tan(δ) over temperature for R-30:70 and the two reference formulations ratios Ref-100:0 and Ref-50:50 (DGEBA instead of DGOA)) .....	50
Figure 31: glass transition temperatures plotted versus acrylate content .....	52
Figure 32: gel content in dependence of the acrylate content.....	54
Figure 33: comparison of rheological measurements under air and nitrogen atmosphere for R- 20:80.....	55
Figure 34: stress relaxation behavior of R-50:50, R-40:60, R-30:70, and R-20:80.....	56
Figure 35: stress relaxation behavior of R-50:50 and the two reference formulations Ref-100:0 and Ref-50:50 (DGEBA instead of DGOA) .....	57
Figure 36: temperature dependent stress relaxation of R-30:70 (a) and Arrhenius plot derived from those measurements (b) .....	59
Figure 37: stress-strain curves for all tested specimens from R-30:70, Ref-100:0, and Ref-30:70. .....	61